

Tidal Venuses: Triggering a Climate Catastrophe via Tidal Heating

Rory Barnes^{1,2,3}, Kristina Mullins^{1,2}, Colin Goldblatt^{1,2,4}, Victoria S. Meadows^{1,2}, James F. Kasting^{2,5}, René Heller⁶

ABSTRACT

Traditionally stellar radiation has been the only heat source considered capable of determining global climate on long timescales. Here we show that terrestrial exoplanets orbiting low-mass stars may be tidally heated at high enough levels to induce a runaway greenhouse for a long enough duration for all the hydrogen to escape. Without hydrogen, the planet no longer has water and cannot support life. We call these planets “Tidal Venuses,” and the phenomenon a “tidal greenhouse.” Tidal effects also circularize the orbit, which decreases tidal heating. Hence, some planets may form with large eccentricity, with its accompanying large tidal heating, and lose their water, but eventually settle into nearly circular orbits (i.e. with negligible tidal heating) in the habitable zone (HZ). However, these planets are not habitable as past tidal heating desiccated them, and hence should not be ranked highly for detailed follow-up observations aimed at detecting biosignatures. We simulate the evolution of hypothetical planetary systems in a quasi-continuous parameter distribution and find that we can constrain the history of the system by statistical arguments. Planets orbiting stars with masses $\lesssim 0.3 M_{\text{Sun}}$ may be in danger of desiccation via tidal heating. We apply these concepts to Gl 667C c, a $\sim 4.5 M_{\text{Earth}}$ planet orbiting a $0.3 M_{\text{Sun}}$ star at 0.12 AU. We find that it probably did not lose its water via tidal heating as orbital stability is unlikely for the high eccentricities required for the tidal greenhouse. As the inner edge of the HZ is defined by the onset of a runaway or moist greenhouse powered by radiation, our results represent a fundamental revision to the HZ for non-circular orbits. In the appendices we review a) the moist and runaway greenhouses, b) stellar mass-radius and mass-luminosity relations, c) terrestrial planet mass-radius relations, and d) linear tidal theories.

¹Astronomy Department, University of Washington, Box 951580, Seattle, WA 98195

²NASA Astrobiology Institute – Virtual Planetary Laboratory Lead Team, USA

³E-mail: rory@astro.washington.edu

⁴Department of Earth and Ocean Science, University of Victoria, Victoria, BC

⁵Department of Geosciences, The Pennsylvania State University, State College, PA

⁶Leibniz Institute for Astrophysics Potsdam

1. Introduction

All life on Earth requires liquid water. Not surprisingly, our search for life on exoplanets therefore begins with identifying environments that support it (Hart 1979; Kasting et al. 1993; Selsis et al. 2007; von Bloh et al. 2007). Many other features of a planet are also important, such as the mix of gases in the atmosphere and the interior’s structure and energy budget, but current research has focused primarily on the stability of surface water. On Earth, liquid water persists primarily because the Sun’s radiation heats the surface to a temperature between water’s freezing and boiling points. Thus, the concept of a “habitable zone” (HZ) emerged, which is the region around a star in which insolation can maintain liquid water on the surface, assuming an Earth-like planet.

Stars have a wide range of luminosities, most of which are considerably lower than the Sun’s, yielding HZs that are closer in. At the extreme, the luminosity becomes so low that even a planet orbiting at the stellar surface would be frozen. Such a star has no HZ. The recently-discovered Y dwarf (which is not a star) WISEP J1828+2650 (Cushing et al. 2011), with an effective temperature below 300 K, is an example of such a primary. For warmer stars, HZs may still be close enough in that non-radiative processes may impact habitability, such as stellar flaring (*e.g.* Lammer et al. 2007; Khodachenko et al. 2007; Tian 2009; Segura et al. 2010; Lammer et al. 2010), decreased volatile inventory (Raymond et al.

2007; Lissauer 2007) or tidal effects (*e.g.* Kasting et al. 1993; Joshi et al. 1997; Jackson et al. 2008a; Correia et al. 2008; Barnes et al. 2009a). As the HZ of our Sun is too distant for these phenomena to affect the Earth, we can only explore their role theoretically, and, consequently, many scientists consider close-in planets less favorable candidates for habitability.

Nevertheless, the last few years have seen renewed interest in the potential habitability of planets in orbit about low luminosity objects (Tarter et al. 2007; Scalo et al. 2007; Lunine et al. 2008; Monteiro 2010; Agol 2011; Bolmont et al. 2011). This shift occurred because terrestrial-sized planets are easiest to detect around low luminosity hosts, due to the larger mass and radius of the planet relative to the star. Furthermore, these objects are the most abundant in the solar neighborhood. Planets with masses between 1 and 10 M_{Earth} , “super-Earths,” have indeed been detected in the last few years around low-mass stars, such as Gl 581 d and Gl 667C c by radial velocity (Udry et al. 2007; Mayor et al. 2009; Vogt et al. 2010; Forveille et al. 2011; Bonfils et al. 2011; Anglada-Escudé et al. 2012; Delfosse et al. 2012) and GJ 1214 b by transit (Charbonneau et al. 2009; Sada et al. 2010; Kundurthy et al. 2011; Carter et al. 2011). Several observational campaigns designed specifically to detect planets around low mass stars are now underway (Nutzman & Charbonneau 2008; Boss et al. 2009; Zechmeister et al. 2009; Bean et al. 2010; Rodler et al. 2011).

The inner edge of the HZ is especially prone to non-radiative phenomena. Traditionally, the inner boundary is defined by the stellar distance at which insola-

(AIP), An der Sternwarte 16, 14482 Potsdam, Germany

tion is strong enough to remove all water in the atmosphere and on the surface (Kasting 1988). Two different dehydrating scenarios (the “moist” and “runaway” greenhouse) are discussed in detail in § 2 and App. A. Both require water vapor to penetrate a stratosphere, be dissociated (photolyzed) by high energy radiation, and culminate in the escape of hydrogen. We call any process that can ultimately lead to total water loss a “desiccating greenhouse.” Without sufficient hydrogen, water cannot form, and the planet will remain uninhabitable forever, unless a major, unlikely event occurs, *e.g.* an impact by a water-rich body that simultaneously delivers water and changes the atmosphere in a way that halts the desiccating greenhouse. This definition of the inner edge is conservative because no known process can maintain habitability against a desiccating greenhouse. Other processes could be equally deleterious for life, but clearly total desiccation will terminate habitability.

We will discuss four types of terrestrial planets in this study, classified by their water content. “Wet” planets are terrestrial exoplanets that have a water content similar to the Earth. “Dry” exoplanets have far less, ~ 3 cm deep if condensed and spread globally, but are habitable (see Abe et al. 2011). “Desiccated” planets have lost all their water through a desiccating greenhouse. Finally, “water worlds,” (Raymond et al. 2004; Léger et al. 2004) are planets with a much larger inventory of water than the modern Earth, *e.g.* a warm Europa. This investigation explores the transition of wet, dry and water worlds into the desiccated state.

Dole (1964) was the first to point out that terrestrial planets in the HZ of low luminosity stars can have their spin altered by tidal interaction. In particular, the danger of synchronous rotation, *i.e.* one hemisphere always facing the star, was emphasized. Kasting et al. (1993) quantified this concept and found that planets orbiting within the HZ of stars less than two-thirds the mass of the Sun were in danger of synchronization. Although their analysis was limited to Earth-like planets on circular orbits, a general belief developed that those planets could not be habitable, as one half of the planet would freeze while the other would roast.

Synchronization is certainly an important consideration when assessing habitability, and many investigations have explored its role, but with mixed results. Atmospheric modeling initially suggested that circulation will transport energy to the unlit side, ameliorating the extreme temperature difference (Joshi et al. 1997). Some subsequent modeling has confirmed that synchronous rotators are likely to have super-rotating atmospheres (Joshi 2003; Heng & Vogt 2011; Edson et al. 2011; Showman & Polvani 2011), while others have discounted it (Wordsworth et al. 2011), and still others have suggested that such a state might be beneficial at the outer edge of the HZ (Pierrehumbert 2011). Taken together, these investigations suggest that synchronized planets should not be dismissed uniformly as uninhabitable. Hence, synchronization is not as stringent a constraint as desiccation, and therefore is not an HZ boundary.

For many years, confusion also existed regarding the term “tidal locking.” Many

investigators assumed it was synonymous with “synchronous rotation.” If the orbits are non-circular, as for many exoplanets (Butler et al. 2006), then tidally-evolved planets may reach an equilibrium state where they rotate faster than synchronous with an “equilibrium” or “pseudo-synchronous” period. This aspect of tidal theory has been known for decades (*e.g.* Goldreich 1966; Greenberg & Weidenschilling 1984), but has only recently been pointed out for the case of exoplanets (Barnes et al. 2008; Ferraz-Mello et al. 2008; Correia et al. 2008). Therefore, some exoplanets, such as Gl 581 d with an eccentricity of 0.38 (Mayor et al. 2009), may be “tidally locked” but rotate about twice per orbit (Barnes et al. 2008; Heller et al. 2011). For more on this point, consult Murray & Dermott (1999), chap. 5.2. In this paper, we use “tidally locked” to mean a planet rotating at the equilibrium period as determined by its eccentricity and obliquity, see Eqs. (D7), (D15)–(D16). In summary, a synchronously rotating planet is tidally locked, but a tidally locked planet is not necessarily rotating synchronously.

Even if an orbit is currently circular, tides may not have driven the rotation to synchronous. If the orbit began with large eccentricity, tides will tend to damp it to zero and we may expect it to be rotating synchronously. However, the planet could pass through one or more “spin-orbit resonances,” where the planet’s rotational frequency is commensurate with its orbital frequency. For example, Mercury rotates three times for every two times it orbits the sun, a 3:2 spin-orbit resonance. Spin-orbit resonances require an inhomogeneous mass distribution, which is likely for tidally-

deformed exoplanets, but cannot be measured for the foreseeable future. A planet caught in a spin-orbit resonance may remain in that state even if circularized, as a resonance is a strong dynamical process. For any particular exoplanet, capture and retention into a spin-orbit resonance will be very difficult to constrain observationally, so all reasonable options should be considered. Therefore, synchronous rotation is unlikely for planets with large eccentricities (Mercury’s is 0.2), and not even guaranteed for a circular orbit. For more on spin-orbit resonances, the reader is referred to Murray & Dermott (1999), chap. 5.4.

As tidal locking of the planetary rotation is not an absolute constraint on habitability, we turn to tidal heating as the other tidal phenomenon most likely to affect planetary habitability. As a planet moves from periastron, its closest approach to the star, to apoastron, the furthest point, and back again, the gravitational force changes, being inversely proportional to distance squared. This difference creates an oscillating strain on the planet that causes it to undergo periodic deformation. The rigidity of the planet resists the deformation, and friction generates heat. This energy production is called tidal heating.

Tidal heating is responsible for the volcanism on Io (Strom et al. 1979; Laver et al. 2007), which was predicted, using tidal theory, by Peale et al. (1979). Io is a small body orbiting Jupiter with an eccentricity of 0.0041, which is maintained by the gravitational perturbations of its fellow Galilean moons, that shows global volcanism which resurfaces the planet on a timescale of $100 - 10^5$ years (Johnson et al.

1979; Blaney et al. 1995; McEwen et al. 2004). The masses of Jupiter and Io are orders of magnitude smaller than a star and terrestrial exoplanet, and thus the latter have a much larger reservoir of orbital and rotational energy available for tidal heating. Moreover, some exoplanets have been found with orbital eccentricities larger than 0.9 (Naef et al. 2001; Jones et al. 2006; Tamuz et al. 2008). Thus, the tidal heating of terrestrial exoplanets may be much more effective than on Io (Jackson et al. 2008c,a; Barnes et al. 2009a, 2010; Heller et al. 2011). This expectation led to the proposition that terrestrial exoplanets with surface heat fluxes as large or larger than Io’s should be classified as “Super-Ios”, rather than “Super-Earths” (Barnes et al. 2009b). Numerous Super-Io candidates exist, such as CoRoT-7 b (Léger et al. 2009; Barnes et al. 2010), Gl 581 e (Mayor et al. 2009), 55 Cnc e (McArthur et al. 2004; Dawson & Fabrycky 2010; Winn et al. 2011), and Kepler-10 b (Batalha et al. 2011), but none is in the HZ.

Jackson et al. (2008a) and Barnes et al. (2009a) considered Io’s heat flux, $\sim 2 \text{ W m}^{-2}$ (Veeder et al. 1994; Spencer et al. 2000; McEwen et al. 2004), to be an upper limit for habitability, arguing that Io-like surfaces are dangerous for habitability. However, 2 W m^{-2} is not sufficient to sterilize a planet, and so should not be considered a hard limit to habitability. For example, the heat flow in inhabited hydrothermal vent systems on Earth, such as the Endeavour segment of the Juan de Fuca Ridge (Holden et al. 1998), is $\sim 30 \text{ W m}^{-2}$ (Fontaine et al. 2011). Thus, a water world with tens of W m^{-2} of energy output could support life. Only if the tidal

heating reached the level to trigger a desiccating greenhouse would habitability be in peril.

Calculations of the inner edge of the HZ have traditionally assumed the primary energy source at the surface is stellar radiation, as is the case for the Earth. Following Barnes et al. (2009a), we call that type of HZ an “insolation HZ” (IHZ), as starlight is the only energy source considered. In this investigation, we identify the amount of tidal heating that triggers a desiccating greenhouse, as well as the combinations of physical and orbital parameters for which tidal heating could yield it. We find such a state is predicted by current models, and dub such a world a “Tidal Venus,” and the phenomenon that produces it a “tidal greenhouse.” The tidal greenhouse would probably have the same effect on habitability as one caused by irradiation, and hence should be considered as hard a limit to habitability as a traditional, insolation-driven desiccating greenhouse.

In this study, we define the limits of Tidal Venuses in terms of stellar and planetary mass, M_* and M_p , respectively, the orbital semi-major axis a , orbital eccentricity e , planetary radius R_p , planetary obliquity ψ_p , and planetary spin frequency ω_p . Some of these quantities are easily observed by current technology, others require special geometries and the next generation of space telescopes. Therefore, for the next decade, not all newly-found planets in an IHZ will have well-constrained tidal heating. This study provides a framework for identifying the range of tidal heating on terrestrial planets orbiting in the IHZ of low luminosity stars. As we see below, the story is complicated and involves

a large parameter space, but is tractable.

We first review the surface conditions that lead to a greenhouse state in § 2, including an extended discussion of the moist and runaway greenhouses (Appendix A), the relationships between mass, radius and luminosity for low-mass, hydrogen burning stars, “M dwarfs” or “late-type stars” in the parlance of astrophysics, and the extent of the IHZ (App. B), and mass-radius relationships for terrestrial exoplanets (App. C). We then briefly describe tidal heating in § 3 with details in App. D. Next we show that tidal heating alone can produce surface conditions capable of triggering a runaway greenhouse on planets orbiting M dwarfs (§ 4). Then we explore how past tidal heating may preclude habitability of planets found in the IHZ regardless of their current tidal heating (§ 5). In § 6 we then consider the Gl 667C system which contains two potentially habitable planets and find that tidal heating is unlikely to have sterilized either. In § 7 we discuss the results, and finally, in § 8 we draw our conclusions.

2. The Inner Edge of the Habitable Zone

Wet planets that are not frozen will always have water vapor in their atmospheres. The amount of water vapor present in equilibrium with a liquid surface is described by the saturation vapor pressure, which depends exponentially on temperature: a warmer planet will have much more water vapor in its atmosphere. Water vapor is a greenhouse gas (see below), so a warmer planet will have a stronger greenhouse effect, enhancing warming, a positive (but not necessarily runaway) feed-

back.

Atmospheric gases on Earth—and those that we expect on habitable Earth-like planets—are mostly transparent to optical wavelengths, so starlight is able to heat the surface. The surface in turn heats the air in contact with it, which rises, expanding and cooling adiabatically. As the air cools, water vapor condenses, releasing latent heat and so slowing the cooling. The net rate of temperature decrease with height is called the “moist adiabatic lapse rate,” setting the mean temperature–pressure (T – p) structure of Earth’s troposphere (the lower region of the atmosphere affected by convection, and bounded at the bottom and top by the planetary surface and the tropopause).

Atmospheric gases which absorb radiation at similar wavelengths to the radiative emission of the planet (thermal infrared for Earth and any habitable planet) are termed “greenhouse gases”; these cause a “greenhouse effect”. The most important greenhouse gases for Earth are water vapor and carbon dioxide. They absorb radiation emitted by the surface, and then re-emit, both downward toward the surface and upward into space. Energy radiated towards the surface (commonly called back radiation) heats the surface. Most importantly, as the atmosphere is cooler than the surface, the amount of radiation emitted to space from the atmosphere is less than the amount of energy emitted by the surface. Thus, the presence of a greenhouse atmosphere means the surface temperature is warmer than the effective temperature of the planet.

Earth’s greenhouse effect keeps the planet warm enough to be habitable; with-

out it Earth’s surface would be at the planet’s effective temperature, a barren 255 K. However, stronger and more water-vapor-rich greenhouse atmospheres can render the planet uninhabitable through high temperature sterilization and/or desiccation (loss of the ocean), and thus define the inner edge of the habitable zone. There are two physically distinct situations that lead to loss of habitability, the “runaway greenhouse” and “moist greenhouse”.

The runaway greenhouse was recently reviewed by Goldblatt & Watson (2012), so we provide a summary description only. As the planet warms, the amount of water vapor in the atmosphere increases such that water becomes a major constituent of the atmosphere and ultimately the dominant one. Consequently, the moist adiabatic lapse rate tends toward the saturation vapor pressure curve for water and the T - p structure of the atmosphere becomes fixed. Concurrently, the atmosphere becomes optically thick in the thermal infrared, such that only the upper troposphere can emit to space. As the T - p structure is fixed, the emitted radiation is also fixed, imposing a limit on the outgoing radiation (F_{crit}) from the troposphere. Values for F_{crit} from the literature are typically 285 W m^{-2} to 310 W m^{-2} for a $1 M_{\text{Earth}}$ planet (Pollack 1971; Watson et al. 1984; Abe & Matsui 1988; Kasting 1988; Pierrehumbert 2010). The physics of this limit is described in more detail in Simpson (1927) and Nakajima et al. (1992). (Komabayashi (1967) and Ingersoll (1969) describe a stratospheric limit at a higher flux, 385 W m^{-2} , which is never reached in practice.) If the amount of energy supplied to the atmo-

sphere by the Sun (Simpson 1927), impacts (Abe & Matsui 1988), or tidal heating (this work) was to exceed F_{crit} then the atmosphere would not be able to maintain radiation balance and runaway heating of the surface would ensue, causing evaporation of the entire ocean. Radiation balance would be regained when either a) the surface temperature reaches $\sim 1400 \text{ K}$ at which point enough radiation is emitted in the near infrared where water vapor is not a good absorber, or b) if water vapor is lost from the atmosphere.

One likely water loss mechanism is hydrogen escape to space. Today, little water vapor reaches the upper atmosphere because the tropopause acts as a “cold trap”: almost all water has condensed lower in the atmosphere, so the tropopause water vapor mixing ratio is low. Water vapor transport above here is generally diffusive, leading to a constant water vapor mixing ratio in the upper atmosphere. (More precisely, in Earth’s atmosphere, water vapor increases with altitude in the stratosphere due to methane oxidation and decreases with altitude in the mesosphere due to photolysis; however, the total hydrogen mixing ratio is conserved, and the hydrogen escape rate depends on this value.) Thus, water is not a strong source of escaping hydrogen and the overall escape rate is low. However, in the runaway greenhouse the atmosphere becomes predominantly water, so no such constraint applies and hydrogen may escape hydrodynamically to space (Kasting & Pollack 1983). The rate will depend on the amount of extreme ultraviolet (EUV) radiation absorbed in the highest part of the atmosphere, so this process is also limited by the available

stellar EUV energy (Watson et al. 1981). A Venus-size planet at the inner edge of the habitable zone, could have lost an ocean the size of Earth’s in $\sim 10^8$ years (Watson et al. 1981); we refer to this as the desiccation time, t_{des} (discussed further below). Deuterium would be retained preferentially over ordinary hydrogen during hydrogen escape. Enrichment of D/H on Venus implies that Venus lost a substantial amount of water to space (Donahue et al. 1982; de Bergh 1993), likely after experiencing a runaway greenhouse.

The moist greenhouse (Kasting 1988) describes a warm atmosphere, in which the whole troposphere is assumed to be water vapor saturated and is underlain by a liquid ocean. As the surface temperature increases, the tropopause is pushed higher (to lower pressure) given the reasonable assumption of a constant tropopause temperature. While the saturation vapor pressure at the tropopause is, by this assumption, constant, the saturation mixing ratio of water at the tropopause (p_{sat}/p_{trop}) increases as the tropopause moves higher. The cold trap is then no longer effective, and substantial water vapor penetrates the stratosphere, and water-derived hydrogen escape can be effective. The planet may thus gradually desiccate while in a hot, but stable, climate. This process could be driven by high greenhouse gas inventories rather than external heating.

A key distinction between the runaway and moist greenhouses is that the former happens when a known flux of energy is supplied to the planet, whereas the latter depends most strongly on surface temperature. Increasing the planet’s inventory of non-condensable greenhouse gases

has a small effect on the runaway greenhouse limit, but can drive the moist greenhouse since the H_2O mixing ratio is lower. Thus, the runaway greenhouse is a more conservative choice to demarcate the inner edge of the IHZ, as knowledge of the atmospheric composition may not be available.

In Fig. 1 we show the moist and runaway greenhouse for wet planets in orbit around M dwarfs. See App. A–C for a discussion of IHZ limits, stellar mass-radius and mass-luminosity relationships, and terrestrial mass-radius relationships. In Fig. 1, the grey regions are the limits of the moist greenhouse as presented in Selsis et al. (2007). At the inner edge, Selsis et al. (2007) find that 300 W m^{-2} triggers the moist greenhouse on a $1 M_{\text{Earth}}$ planet, and, from left to right, the limits assumed 100%, 50% and 0% cloud cover (for a $0.25 M_{\text{Sun}}$ star these limits correspond to bond albedos of 0.75, 0.49 and 0.23, respectively). The solid curve is the runaway greenhouse limit (Pierrehumbert 2010) for a $30 M_{\text{Earth}}$ planet and dashed for a $0.3 M_{\text{Earth}}$ planet, both with an albedo of 0.49 (compare to the medium grey). As expected (see App. A) the smaller planet’s inner edge lies at larger semi-major axis than both $1 M_{\text{Earth}}$ moist greenhouse limit, which in turn lies farther out than the $30 M_{\text{Earth}}$ runaway greenhouse limit.

We have presented the classical description of the desiccation at the inner edge of the habitable zone above. Various complications are worthy of note. Water on a dry planet will get trapped at the poles, making a moist or runaway greenhouse harder to achieve and meaning that the inner edge of the HZ is nearer the star (Abe et al. 2011). We do not include that limit in

Fig. 1 but we return to it in § 4. Fig. 1 assumes the planetary orbit is circular. However, for the many exoplanets with (highly) eccentric orbits (Butler et al. 2006), the total irradiation over an orbit determines the annual-averaged surface temperature (Williams & Pollard 2002) and pushes the IHZ boundaries out by a factor of $(1 - e^2)^{-1/4}$ (Barnes et al. 2008).

Regarding the desiccation time, 10^8 yr from energy limited hydrogen escape for a Venus-like planet is used throughout as the best available number, but there are various unknowns which may affect this value. The masses of exoplanet oceans are unknown. Earth’s mantle contains a few ocean masses of water (Bell & Rossman 1992; Murakami et al. 2002; Marty & Yokochim 2006), so it is possible that the surface of a planet could acquire a new ocean after being desiccated, and become habitable again. Very low mass M dwarfs are very active and emit strongly in the near UV, especially when they are young (*e.g.* West et al. 2008), but the total flux is still less than the present-day Sun (Fleming et al. 1993) and the EUV flux (which drives hydrodynamic escape) is not well known.

3. Tidal Heating

Tidal heating is responsible for the volcanic activity on Io (Peale et al. 1979), and probably the geysers of Enceladus (Hansen et al. 2006; Porco et al. 2006; Hurford et al. 2007). Tidal theory has a long and established body of work, however tidal processes remain poorly understood. The difficulty lies in the complexity of the energy dissipation processes and the very long timescales associated with tidal

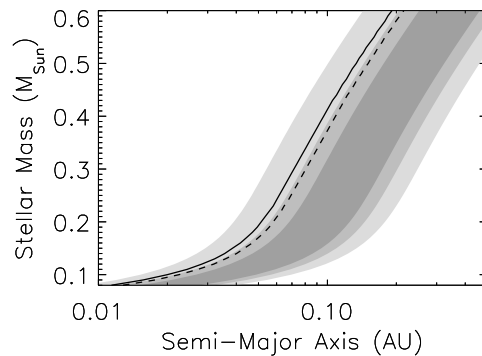


Fig. 1.— Comparison of HZ boundaries for different planetary masses and desiccating greenhouses. The shaded regions represent the IHZ boundaries from Selsis et al. (2007): Dark gray assumes no cloud coverage, medium gray 50%, and light gray 100%, and assuming $1 M_{\text{Earth}}$ planet. The black curves represent the runaway greenhouse limit from Pierrehumbert (2011). The solid curve is for a $30 M_{\text{Earth}}$ planet, dashed for a $0.3 M_{\text{Earth}}$ planet. For these calculations we used the stellar mass-radius relationship from BO06, the mass-luminosity relationship from RH00, and the terrestrial mass-radius relationship from Sotin et al. (2007).

evolution. The Earth-Moon system is the most accurately studied, with lunar laser ranging providing a precise measurement of the recession of the Moon due to tides of ~ 38 mm/yr (Dickey et al. 1994), as well as direct measurements of the locations of dissipation in the ocean (Egbert & Ray 2000). However, extrapolating backwards in time predicts that the Moon was at the Earth’s surface about ~ 2 Gyr ago (MacDonald 1964), which contradicts the standard impact model for the lunar origin (note that numerous issues remain such as the origin of the Earth and Moon’s obliquities (Touma & Wisdom 1994) and the perturbations from other planets (Ćuk 2007)). The deceleration of Io’s orbital velocity has also been tentatively detected and seems broadly consistent with tidal theory (Aksnes & Franklin 2001; Lainey et al. 2009). However, these data lie in the same regime, that of nearly-circular orbits. Exoplanets have been found with extremely eccentric orbits, so we can only extrapolate from our Solar System cautiously. The details of tidal theory are complicated, and hence we relegate the discussion to App. D.

Two end-member models of tides theory have been applied to exoplanets and the bodies of our Solar System: One assumes the energy dissipation gives a constant phase lag in the periodic distortion (CPL), and the other assumes a constant time lag (CTL) (Greenberg 2009). While simple and linear, such models are probably commensurate with the dearth of information we have about exoplanet interior processes. More complicated models have been constructed, and they reproduce the above models for certain choices of internal composition, structure, and energy trans-

port (*e.g.* Henning et al. 2009). Results based on these models should not be considered predictive in individual cases, but they can paint a qualitative picture of rotational and orbital evolution.

These models converge at $e = 0$, and have been shown to be nearly identical for $e \lesssim 0.2$ (Leconte et al. 2010), and when using Eq. (D17). However, for $e \gtrsim 0.4$, they diverge significantly. We urge caution when interpreting results in the upcoming sections which allow e to be as large as 0.8. We include this range primarily for illustrative purposes, and as a baseline for any future work which may include non-linear effects.

The tidal heating of a body is provided in Eqs. (D6) and (D14) for the CPL and CTL models, respectively. Averaging the heating rate of the entire planetary surface gives the surface energy flux due to tides, F_{tide} . In those equations, the strength of the tidal effects is parameterized as a “tidal quality factor” Q (CPL) or “tidal time lag” τ (CTL), which are notoriously difficult to measure or estimate from first principles. The Earth’s current values are $Q = 12$ (Yoder 1995) and $\tau = 638$ s (Lambeck 1977; Neron de Surgy & Laskar 1997), respectively. However, as noted above, these values predict too short a lifetime of the Moon. This discrepancy has led to the notion that the Earth’s response to lunar tides has evolved with time, possibly due to changing size, shape and bathymetry of the oceans, affecting the ocean currents response to the tidal potential. Measurements of the dry bodies in our Solar System have found that their Q s tend to cluster around 100, see App. D.

Recent satellite observations of the

Earth have revealed the locations of tidal dissipation in our oceans (Egbert & Ray 2000). Tides force water through shallow seas and straits causing energy dissipation. In the open ocean, tidal dissipation is probably a non-linear process in which currents are disrupted by seafloor topography. The presence of the ocean provides more opportunity for tidal dissipation than on dry planets. Therefore, for the following calculations we assume modern Earth-like planets with $Q = 10$ or $\tau = 640$ s.

4. Tidal Venuses

We computed tidal heating rates for a range of planetary, stellar and orbital parameters and find that tidal heating can be strong enough on some planets to trigger a runaway greenhouse. In Fig. 2 we show the configurations that predict this state around 4 different M dwarfs. The IHZ boundaries are the moist greenhouse limits from Selsis et al. (2007) and with the same format as Fig. 1. The colored curves mark where $F_{tide} = F_{crit}$. Red curves assume the CTL model, blue the CPL with discrete rotation states, see App. D.1. Solid curves assume the Pierrehumbert (2011) runaway greenhouse model, and dotted the dry world model of Abe et al. (2011), *c.f.* Fig. 6 in App. A. Thick lines are for a $10 M_{\text{Earth}}$ planet, and thin for $1 M_{\text{Earth}}$ (Abe et al. (2011) only considered a $1 M_{\text{Earth}}$ planet). Note that our choice for the relationship between Q and τ influences which model predicts more heating. If we had chosen the same relationship as in Heller et al. (2011), we would have found the CTL model predicts more heating than CPL, *c.f.* their Fig. 5.

For the lowest mass M dwarfs, the IHZ

is significantly reduced due to tidal heating. For masses larger than $0.25 M_{\text{Sun}}$, a tidal greenhouse in the IHZ is only possible on large mass planets with very large eccentricities. Note that our model predicts a tidal greenhouse at low eccentricities where tidal theory is most likely valid. Figure 2 shows that a planet may have a climate catastrophe due to tide-driven overheating even if it is far enough from the star that stellar radiative heating alone would not preclude habitability.

The difference between curves representing equal mass planets is due to the frequency dependence of the CTL model. For the Earth, the frequency is the mean motion of the lunar orbit, but a planet at $a = 0.035$ AU, *i.e.* the middle of the HZ, orbits in about 1 week. One could adjust τ so that it is equivalent to a Q of 100 ((see *e.g.* Matsumura et al. 2010; Heller et al. 2011) and Eq. [D17]) and then the curves would be lie in a similar location. The true nature of terrestrial exoplanets is unknown, and thus we have arbitrarily adopted modern Earth values for all planets at all frequencies.

Regions to the left of the colored curves in Fig. 2 can produce Tidal Venuses if the planets remain there longer than t_{des} . In Fig. 3, we show the evolution of an example system of a $10 M_{\text{Earth}}$ planet orbiting a $0.1 M_{\text{Sun}}$ star, assuming the CPL model. The planet begins with semi-major axis $a = 0.04$ AU, and $e = 0.3$. This orbit is toward the outer edge of the IHZ and with the typical eccentricity of known exoplanets. The top panel shows the evolution of a (note that for this configuration the CPL model predicts a will increase), the next panels down show e , then insolation F_{insol}

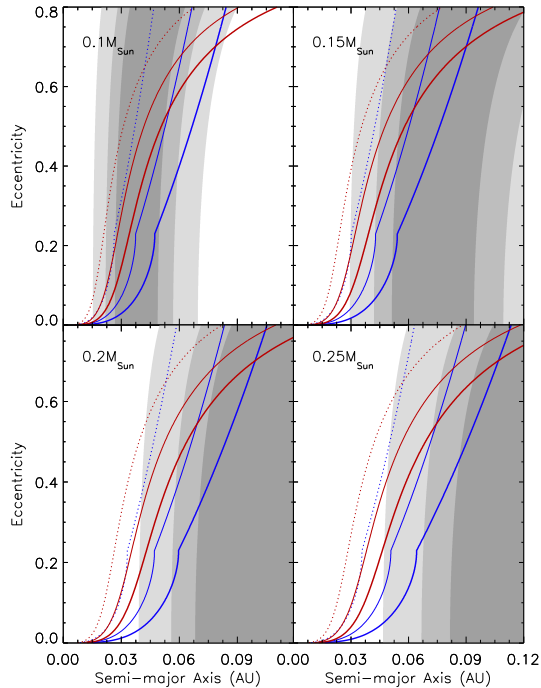


Fig. 2.— Parameter space of the Tidal Venus. The top left panel is a $0.1 M_{\text{Sun}}$ star, top right $0.15 M_{\text{Sun}}$, bottom left $0.2 M_{\text{Sun}}$, and bottom right $0.25 M_{\text{Sun}}$. The grayscale represents the Selsis et al. (2007) IHZ boundaries: From lightest to darkest gray, the cloud coverage is 100%, 50% and 0%, respectively. The colored curves mark where $F_{\text{tide}} = F_{\text{crit}}$. Red curves assume the CTL model, blue the CPL. Solid curves assume the (Pierrehumbert 2011) runaway greenhouse model, and dotted the dry world model of (Abe et al. 2011). Thick lines are for a $10 M_{\text{Earth}}$ planet, and thin for $1 M_{\text{Earth}}$. Tidal Venuses lie to the left of these curves.

and finally tidal heat flux. The planet is assumed to be spin-locked and with zero obliquity. The flux received by the planet has decreased to $F_{\text{crit}} = 345 \text{ W m}^{-2}$ at 200 Myr, and the sum of tidal heating and insolation reaches F_{crit} at 275 Myr. Therefore, planets orbiting low-mass stars on eccentric orbits may experience tidal greenhouse conditions long enough to be uninhabitable.

5. Constraining Observed Planets

The previous section demonstrated that planets may become desiccated by tidal heating, but in many cases we will be more interested in the possibility that such a condition developed on a planet that we have discovered. As tides tend to circularize orbits, we may find a planet in the IHZ with low eccentricity that experienced a tidal greenhouse early on and is hence currently uninhabitable. In this section we describe how to evaluate a known planet’s probability for habitability based on past tidal heating.

In order to evaluate the tidal heating history of an exoplanet, we require knowledge of M_p , R_p , a , e , M_* , R_* and age. Exoplanets are predominantly discovered by RV and transit studies that can provide a and e , while the others can be modeled from the stellar spectrum. If some of these values are unknown, we can often use scaling relations to estimate them, see App. B–C. From this information, one can estimate the tidal heating history of a planet, using the tidal evolution equations (App. D), and hence estimate the probability that the planet has lost its water.

To explore this issue, consider a hypothetical situation in which a terrestrial-

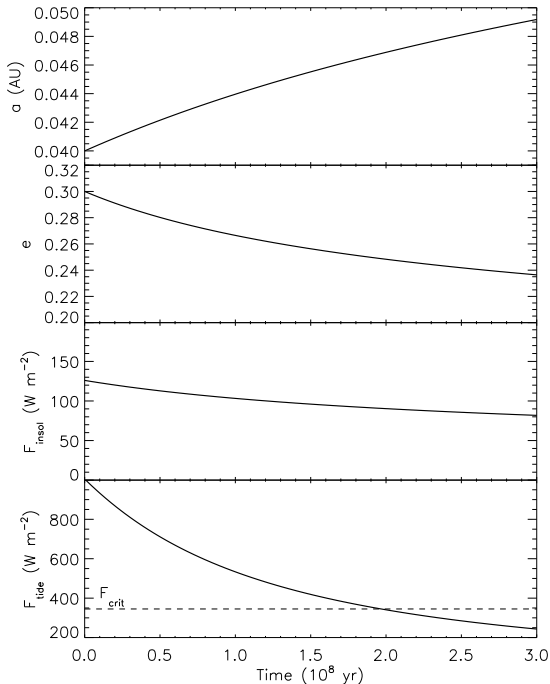


Fig. 3.— Evolution of a $10 M_{\text{Earth}}$ planet orbiting a $0.1 M_{\text{Sun}}$ star with an initial orbit of $a = 0.04$ AU, $e = 0.3$. *Top*: Semi-major axis evolution. *Top middle*: Eccentricity evolution. *Bottom Middle*: Insolation evolution. *Bottom*: Tidal heat flux evolution.

scale planet has been discovered in orbit about an M dwarf. Further, the planet lies near the inner edge of the IHZ, and has a low eccentricity. To evaluate past tidal heating, we created 4 systems with different stellar and planetary properties, applied reasonable uncertainties to each observable properties, chose non-observable properties via appropriate scaling laws, and modeled the system’s history. In particular, we assume that the planet’s mass lies between 1 and 5 M_{Earth} , has an eccentricity less than 0.1, a tidal Q_p (τ_p) in the range 10 – 100 (640 – 64 s), and is tidally-locked. We assume the star’s age lies between 2 and 8 Gyr, and Q_* (τ_*) in the range $10^5 - 10^{10}$ ($1 - 10^{-4}$ s) and $t_{des} = 10^8$ years. We used the same scaling relations as above. For the $0.1 M_{\text{Sun}}$ case, a was chosen in the range [0.029,0.031] AU, for $0.15 M_{\text{Sun}}$ it was [0.055,0.065] AU, for $0.2 M_{\text{Sun}}$ it was [0.085,0.095] AU, and for $0.25 M_{\text{Sun}}$ it was [0.095,0.105] AU. For each parameter the uncertainty distribution was uniform in the quoted range, except for e which was chosen uniformly in the range $-5 \leq \log_{10}(e) \leq -1$. We then randomly determined the system parameters in these ranges and integrated the tidal history backward in time, using the models presented in App. D, for the randomly chosen age of the system. For each stellar mass and tidal model, we simulated 30,000 possible configurations.

In Fig. 4 we show our results graphically. As we are considering a range of masses, we choose to represent the runaway greenhouse flux with a $2.5 M_{\text{Earth}}$ planet, *i.e.* the solid curves show where $F_{tide} = F_{crit} = 309 \text{ W m}^{-2}$. The three contours show the probability density for

the planet’s location $t_{des} = 10^8$ years after the system’s formation. The contours show where the probability has dropped by 50%, 90% and 99% of the peak value, solid contours are for the CPL model, dashed for the CTL. If the probability contours intersect, or even come close to, the colored $F_{tide} = F_{crit}$ curves, then the planet may be a “Habitable Zone Venus,” a planet that appears habitable by the IHZ metric, but is probably more Venus-like than Earth-like.

For the $0.1 M_{Sun}$ case (top left), the planet may have spent enough time in the tidal greenhouse to be uninhabitable. For larger mass stars, however, the danger of a tidal desiccation is smaller. In the $0.15 M_{Sun}$ case, the peak in the CPL probability density at $a = 0.08$, $e = 0.45$ represents 1% of our simulations. Although the contours do not cross the CPL runaway greenhouse (blue) curve, they do come close, and hence there is a small chance that our putative candidate is a super-Venus, especially if we allow for absorption of stellar radiation.

However, for $M_* > 0.15 M_{Sun}$, planets with low eccentricity probably have always had low eccentricity, *i.e.* the evolution was negligible. This sharp contrast between 0.1 and $0.2 M_{Sun}$ occurs because of the steep dependence of tidal heating on a . At larger stellar masses, the circular IHZ has been pushed away from the reach of fatal tidal heating.

This experiment is purely illustrative with arbitrary parameters and uncertainty distributions. If a terrestrial planet was discovered in the IHZ of a very low mass star, then this methodology could be performed in order to characterize its potential to support life. One could derive a

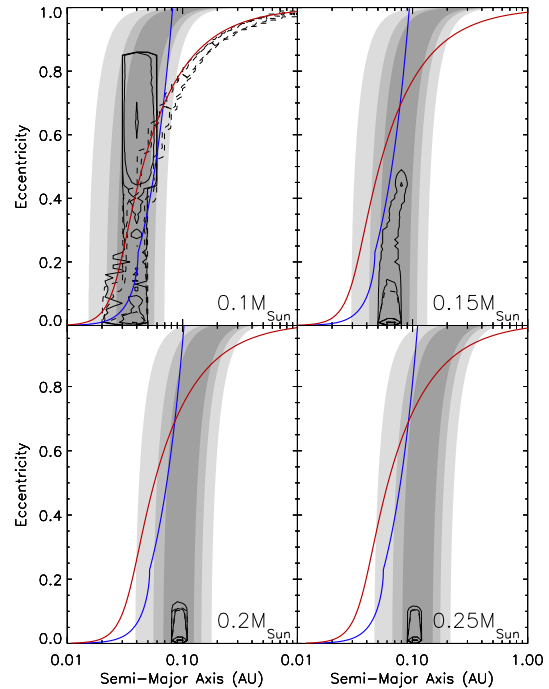


Fig. 4.— Orbits of hypothetical planets around M dwarfs after t_{des} . The top left panel is a $0.1 M_{Sun}$ star, top right $0.15 M_{Sun}$, bottom left $0.2 M_{Sun}$, and bottom right $0.25 M_{Sun}$. The grayscale represents the (Selsis et al. 2007) IHZ boundaries with the same format as Fig. 2. For reference, the red and blue curves show the locus of orbits for which tidal heating of a $2.5 M_{Earth}$ planet with $Q_p = 10$ (CPL model, blue curve) or $\tau_p = 640$ s (CTL model, red curve), assuming the (Pierrehumbert 2011) runaway greenhouse limit. Contours denote levels of constant probability density (for densities 50%, 90% and 99% of the peak value) for the initial orbit of the planet: solid corresponds to the CPL model (compare to blue curve), dashed to CTL (compare to red curve). In the bottom two panels there has been negligible orbital evolution for either tidal model.

value of t_{des} tailored to the primary, and determine the probability that the planet spent more than that in a tidal greenhouse state and hence is uninhabitable. In principle, one should also allow a range of albedos and include radiation to determine the amount of time that the total surface energy flux, $F_{tot} = F_{tide} + F_{insol}$, is larger than F_{crit} , but we leave such an analysis for future work.

6. Application to Gl 667C

Two or more planets orbit the $0.3 M_{Sun}$ star Gl 667C (Bonfils et al. 2011; Anglada-Escudé et al. 2012; Delfosse et al. 2012). Planets c and d appear to lie in the IHZ, while a third planet, b, lies interior. Planet c is at least $4.25 M_{Earth}$ and orbits near the inner edge of the IHZ. Planet d, which is weakly detected in both studies, lies near the 50% cloud cover outer boundary. At 0.23 AU, planet d is too far from the star to be subjected to strong tidal heating, at least if it is tidally locked. Anglada-Escudé et al. (2012) and Delfosse et al. (2012) propose different solutions to the system with the former setting c’s eccentricity to 0, but stating that it is only constrained to be < 0.27 , while the latter assign its eccentricity to be 0.34 ± 0.1 . The minimum mass estimates are almost identical at $4.25 M_{Earth}$ (Anglada-Escudé et al. 2012) and $4.5 M_{Earth}$ (Delfosse et al. 2012). Here, we use the Delfosse et al. (2012) solution, but note that using data from (Anglada-Escudé et al. 2012) does not change our results.

In Fig. 5, we show the system in the same format as Fig. 2. As this planet was detected via radial velocity data, its true mass is unknown. We consider two possibilities here, an edge-on geometry in which

its actual mass is $4.25 M_{Earth}$ and an inclined case in which its actual mass is doubled, $8.5 M_{Earth}$. In Fig. 5, the thin lines correspond to the minimum mass, thick to twice-minimum. The extent of the line corresponds to the 3σ uncertainty. The orbit of c is marked by the vertical black line at $a = 0.123$ AU, and d at 0.23 AU.

The CTL model (red curves) barely intersect the 100% cloud cover IHZ at large e . The CPL model penetrates the IHZ more significantly, but still does not reach the orbit of c. Thus, planet c is not currently experiencing a tidal greenhouse, assuming no obliquity and pseudo-synchronous rotation. We also see that d is completely safe from the tidal greenhouse.

But could planet c have been in the tidal greenhouse and be desiccated today? The answer is almost assuredly no. In this case, we can appeal to the orbital architecture, rather than running a suite of Monte Carlo simulations as in § 5. The dashed, black line of Fig. 5 showed where the orbit of c crosses the orbit of b. Such a configuration is as close as the two planets could possibly be and remain stable, assuming no mean motion resonances, which are not detected in this system (Anglada-Escudé et al. 2012). This black curve is always exterior to the tidal greenhouse curves out to the current orbit of c. Therefore, we may safely conclude that c was never in a tidal greenhouse due to its orbit. Furthermore, the planet should have become tidally-locked within 10^7 years (Heller et al. 2011), which is much less than t_{des} . Hence any initial burst of tidal heating due to non-equilibrium rotation or obliquity was too short to sterilize this planet. Gl 667C c remains a habitable

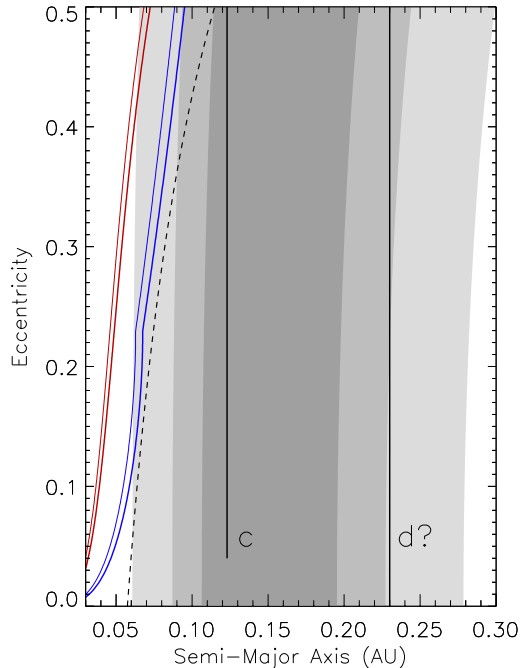


Fig. 5.— Comparison of the IHZ to the tidal greenhouse limits for Gl 667C c, in a similar format as Fig. 2. Here the thin lines correspond to a $4.5 M_{\text{Earth}}$ planet, and thick to $9 M_{\text{Earth}}$. The vertical black lines correspond to the possible orbits of c and d (whose existence remains uncertain). The dashed, black curve represents where c' and b's orbits cross, and hence the region to the left is dynamically unstable.

planet candidate.

7. Discussion

The previous results show where tidal heating can limit habitability for planets orbiting low mass stars. However, many phenomena complicate the process and could alter our findings. Here we discuss the results of the previous sections in light of our simplifying assumptions, observational requirements, and theoretical limitations.

We find that Gl 667C c probably did not lose its water to tidal heating because interactions with other planets prevent its eccentricity from being large enough to trigger the tidal greenhouse. However, as more potentially habitable planets are discovered around low mass stars, a similar analysis as in § 5 should be undertaken in order to assess the possibility that the planet could in fact be dehydrated. As we may only be able to spectroscopically characterize a few planets with the *James Webb Space Telescope* (Seager et al. 2009; Kaltenegger & Traub 2009), prioritization of targets is crucial, and past and present tidal heating will help determine the best planet to observe.

The timescale for e to decay may be smaller than the timescale for in situ terrestrial planet formation (Lecar & Aarseth 1986; Wetherill & Stewart 1989; Lissauer 1993; Kokubo & Ida 1998; Raymond et al. 2007). On the other hand, terrestrial planets could be pushed into such a position by a migrating gas giant in about that timescale (Raymond et al. 2006; Mandell et al. 2007). It is therefore natural to wonder if such planets can even form, as the tidal effects could suppress planet

formation, or damp out the eccentricity of a protoplanet before it is massive enough to support clement conditions. Several scenarios suggest that fully-formed planets can be Tidal Venuses. Orbital instabilities can excite e . Planet-planet scattering and divergent resonance crossing appear to play a role in sculpting many planetary systems, including our own (*e.g.* Weidenschilling & Marzari 1996; Tsiganis et al. 2005; Nesvorný 2011). These phenomena can develop long after planet formation has occurred. Recently it has been suggested that exoplanetary systems in resonance appear systematically younger than the general population, suggesting that instabilities can even occur after many billions of years (Koriski & Zucker 2011). Therefore, we conclude that tidal greenhouses are plausible.

The role of oceans in the tidal dissipation process is clearly very important, yet also very poorly understood. We have used up-to-date information regarding the dissipation of energy in the Earth’s ocean and assumed that terrestrial exoplanets will behave similarly, yet many issues remain outstanding. We have ignored the role of inertial waves, which provide additional heating of aqueous mantles of icy satellites (Tyler 2008, 2011). Therefore the tidal heating values we obtained may, in fact, be too low, further increasing the threat to habitability. Regardless, our choices of Q or τ were rigid, but a wide range of values is possible, as they are complex functions of ocean depth, ocean floor topography and the shape of any continents or islands that may be present. As “exobathymetry” seems a distant dream, tidal

dissipation in Earth-like worlds will remain mysterious for the foreseeable future.

Further complicating the situation, oceans may evaporate long before t_{des} , potentially leading to a cyclical process of evaporation and precipitation: After the oceans disappear, Q increases and the tidal heat decreases, causing the planet to drop out of the tidal greenhouse, so the water rains out, reforming the oceans and lowering Q again. Whether such a cycle exists is pure speculation, but we note that an analogous situation can occur with the classic IHZ, where evaporated water forms clouds that increase the albedo, which in turn lowers the upward long-wavelength flux from the surface, and the planet then drops out of the runaway greenhouse. Our choices for Q , τ , F_{crit} and t_{des} can be revised as new observations provide firmer constraints. Of these, t_{des} needs the most work, as it is a function of poorly constrained host properties, and challenging planetary escape processes, see *e.g.* Tian (2009)

A Tidal Venus is an extreme case of tidal heating, over two orders of magnitude more powerful than on Io. We have therefore made a considerable extrapolation. Perhaps oceans and/or mantles adjust to the increased heating and fail to reach that flux. Our choice for Q and τ imply most dissipation occurs in the ocean. For the solid interior, Běhouňková et al. (2011) find that tidal heating at about F_{crit} leads to a “thermal runaway” for planets that transport internal energy through convection. Although they did not consider the possibility of advection via volcanism, the geophysics of Tidal Venuses require closer scrutiny. We are unaware of any research exploring the physical oceanography of

planets undergoing strong tidal heating, suggesting it is an interesting topic for future research.

Our treatment ignored mutual gravitational interactions between planets, which can significantly alter the evolution. Gravitational perturbations can pump up eccentricities and obliquities to non-zero values and may be able to modify the spin period. From Fig. 2, we see that planets near the inner edge of the HZ may be in a tidal greenhouse for eccentricities less than 0.02. Other bodies in the system can easily perturb eccentricities to larger values, hence planets in multiple systems may be especially susceptible to a tidal greenhouse, as this driven eccentricity can be maintained for arbitrarily long timescales. As individual systems are discovered, this point should be revisited.

On the other hand, orbital stability arguments could allow us to preclude the tidal greenhouse in multiplanet systems, as for Gl 667C. When the eccentricity required for the tidal greenhouse is so large that the system is unstable, then one can safely exclude the Tidal Venus state. Hence, the presence of additional companions provides critical information when assessing habitability.

Many other critical phenomena were also left out such as atmospheric erosion by flaring, stellar activity and magnetic dynamo generation (Lammer et al. 2007; Khodachenko et al. 2007; Tian 2009; Segura et al. 2010; Lammer et al. 2010; Driscoll & Olson 2011). Tidal heating provides an interesting counterbalance to atmospheric erosion as it may increase the outgassing rates and maintain a permanent atmosphere. The outgassing and es-

cape need to remain in a balance as wild pressure and density fluctuations will undoubtedly alter the biosphere, but in principle, tidally-driven outgassing could reduce the danger of atmospheric removal. On the other hand, more intense outgassing without commensurate draw down by processes like the carbonate-silicate cycle could increase the threat of a moist greenhouse. Magnetic fields may slow down atmospheric loss, but tidal heating may decrease the dynamo. If magnetic fields are generated by convection in the outer core between a hot inner core and a cool mantle (Olson & Christensen 2006; Driscoll & Olson 2011), then tidal heating of the mantle may suppress magnetic field generation (Stevenson 2010). This issue has not yet been explored for tidally-heated exoplanets, but it could play a major role in habitability. Future work should couple outgassing and escape rates in order to determine how the two interact.

8. Conclusions

We have shown that tidal heating of some exoplanets may exceed the threshold of the runaway greenhouse, the traditional inner edge of the IHZ. We find that for stars with masses $\lesssim 0.3 M_{\text{Sun}}$, planets in their IHZs with low eccentricity, can be uninhabitable regardless of insolation. We have thus fundamentally revised the HZ boundaries for planets on eccentric orbits. Unlike insolation from main sequence stars, tidal heating at a desiccating greenhouse level may drop off rapidly, but not so rapidly as to preclude the possibility that a planet's entire inventory of water can be lost permanently, see Fig. 3. These planets will be uninhabitable regardless of fu-

ture tidal heating, *i.e.* a planet found with minimal tidal heating today may still have experienced sufficient heating for sufficient duration to render the planet uninhabitable. Additional planetary companions are important: They can drive eccentricity and sustain a tidal greenhouse, or they can be used with stability arguments to rule out an early tidal greenhouse.

Traditionally, habitability models have focused on insolation, implying the star is the most important aspect of habitability. We have shown that in some circumstances tidal effects are more important in determining the inner edge of the HZ. Planetary habitability is a function of the star, the planet, and the planetary system (Meadows et al. in prep.). The Kasting et al. (1993) IHZ has served well as a guide, but is insufficient. Combining all the processes relevant to habitability into a single model is a daunting challenge to say the least, but a proper assessment of a planet's potential for habitability relies on a wide diversity of properties, some of which will not be observable any time soon. Nevertheless, the prospect of identifying an inhabited planet is strong motivation. Moreover, the high cost in time, money and resources required to establish a planet as inhabited demand that we use these resources efficiently. In this study we have compiled numerous tidal processes and empirical relationships so that at least the tidal effects predicted by linear theory may be applied to terrestrial planets in the IHZs of low luminosity hosts.

This work was funded by NASA Astrobiology Institute's Virtual Planetary Laboratory lead team, under cooperative agreement No. NNH05ZDA001C. RB ac-

knowledges additional funding from NSF grant AST-1108882. We are also grateful for stimulating discussions with Richard Greenberg, Norm Sleep, Sean Raymond, and Andrew Rushby.

REFERENCES

- Abe, Y., Abe-Ouchi, A., Sleep, N. H., & Zahnle, K. J. 2011, *Astrobiology*, 11, 443
- Abe, Y., & Matsui, T. 1988, *J. Atmos. Sci.*, 45, 3081
- Adams, E. R., López-Morales, M., Elliot, J. L., Seager, S., & Osip, D. J. 2011, *Astrophys. J.*, 728, 125
- Agol, E. 2011, *Astrophys. J.*, 731, L31+
- Aksnes, K., & Franklin, F. A. 2001, *Astron. J.*, 122, 2734
- Anglada-Escudé, G. et al. 2012, ArXiv e-prints
- Baraffe, I., Chabrier, G., Allard, F., & Hauschildt, P. H. 1998, *Astro. & Astrophys.*, 337, 403
- Barnes, R., Jackson, B., Greenberg, R., & Raymond, S. N. 2009a, *Astrophys. J.*, 700, L30
- Barnes, R., Jackson, B., Raymond, S. N., West, A. A., & Greenberg, R. 2009b, *Astrophys. J.*, 695, 1006
- Barnes, R., Raymond, S. N., Greenberg, R., Jackson, B., & Kaib, N. A. 2010, *Astrophys. J.*, 709, L95
- Barnes, R., Raymond, S. N., Jackson, B., & Greenberg, R. 2008, *Astrobiology*, 8, 557

- Batalha, N. M. et al. 2011, *Astrophys. J.*, 729, 27
- Bayless, A. J., & Orosz, J. A. 2006, *Astrophys. J.*, 651, 1155
- Bean, J. L., Seifahrt, A., Hartman, H., Nilsson, H., Wiedemann, G., Reiners, A., Dreizler, S., & Henry, T. J. 2010, *Astrophys. J.*, 713, 410
- Bell, D. R., & Rossman, G. R. 1992, *Science*, 255, 1391
- Bills, B. G., Neumann, G. A., Smith, D. E., & Zuber, M. T. 2005, *Journal of Geophysical Research (Planets)*, 110, E07004
- Blaney, D. L., Johnson, T. V., Matson, D. L., & Veeder, G. J. 1995, *Icarus*, 113, 220
- Bolmont, E., Raymond, S. N., & Leconte, J. 2011, ArXiv e-prints
- Bond, J. C., O'Brien, D. P., & Lauretta, D. S. 2010, *Astrophys. J.*, 715, 1050
- Bonfils, X. et al. 2011, ArXiv e-prints
- Boss, A. P. et al. 2009, *Pub. Astron. Soc. Pac.*, 121, 1218
- Butler, R. P. et al. 2006, *Astrophys. J.*, 646, 505
- Běhounková, M., Tobie, G., Choblet, G., & Čadež, O. 2011, *Astrophys. J.*, 728, 89
- Carone, L., & Pätzold, M. 2007, *Plan. & Sp. Sci.*, 55, 643
- Carter, J. A., Winn, J. N., Holman, M. J., Fabrycky, D., Berta, Z. K., Burke, C. J., & Nutzman, P. 2011, *Astrophys. J.*, 730, 82
- Charbonneau, D. et al. 2009, *Nature*, 462, 891
- Correia, A. C. M., & Laskar, J. 2001, *Nature*, 411, 767
- . 2003, *Journal of Geophysical Research (Planets)*, 108, 5123
- Correia, A. C. M., Levrard, B., & Laskar, J. 2008, *Astro. & Astrophys.*, 488, L63
- Čuk, M. 2007, *Science*, 318, 244
- Cushing, M. C. et al. 2011, ArXiv e-prints
- Darwin, G. H. 1880, *Royal Society of London Philosophical Transactions Series I*, 171, 713
- Dawson, R. I., & Fabrycky, D. C. 2010, *Astrophys. J.*, 722, 937
- de Bergh, C. 1993, *Origins of Life and Evolution of the Biosphere*, 23, 11
- Delfosse, X. et al. 2012, ArXiv e-prints
- Dickey, J. O. et al. 1994, *Science*, 265, 482
- Dole, S. H. 1964, *Habitable planets for man*
- Donahue, T. M., Hoffman, J. H., Hodges, R. R., & Watson, A. J. 1982, *Science*, 216, 630
- Driscoll, P., & Olson, P. 2011, *Icarus*, 213, 12
- Edson, A., Lee, S., Bannon, P., Kasting, J. F., & Pollard, D. 2011, *Icarus*, 212, 1

- Efroimsky, M., & Lainey, V. 2007, *Journal of Geophysical Research (Planets)*, 112, E12003
- Efroimsky, M., & Williams, J. G. 2009, *Celestial Mechanics and Dynamical Astronomy*, 104, 257
- Egbert, G. D., & Ray, R. D. 2000, *Nature*, 405, 775
- Ferraz-Mello, S., Rodríguez, A., & Hussmann, H. 2008, *Celestial Mechanics and Dynamical Astronomy*, 101, 171
- Fischer, H.-J., & Spohn, T. 1990, *Icarus*, 83, 39
- Fleming, T. A., Giampapa, M. S., Schmitt, J. H. M. M., & Bookbinder, J. A. 1993, *Astrophys. J.*, 410, 387
- Fontaine, F. J., Olive, J.-A., Cannat, M., Escartin, J., & Perol, T. 2011, *Geophys. Res. Lett.*, 381, 14307
- Fortney, J. J., Marley, M. S., & Barnes, J. W. 2007, *Astrophys. J.*, 659, 1661
- Forveille, T. et al. 2011, *ArXiv e-prints*
- Garrett, C., & Kunze, E. 2007, *Annual Review of Fluid Mechanics*, 39, 57
- Gold, T., & Soter, S. 1969, *Icarus*, 11, 356
- Goldblatt, C., & Watson, A. J. 2012, *ArXiv e-prints*
- Goldreich, P. 1966, *Astron. J.*, 71, 1
- Goldreich, P., & Soter, S. 1966, *Icarus*, 5, 375
- Gorda, S. Y., & Svechnikov, M. A. 1999, *Astronomy Reports*, 43, 521
- Grasset, O., Schneider, J., & Sotin, C. 2009, *Astrophys. J.*, 693, 722
- Greenberg, R. 2009, *Astrophys. J.*, 698, L42
- Greenberg, R., & Weidenschilling, S. J. 1984, *Icarus*, 58, 186
- Hansen, C. J., Esposito, L., Stewart, A. I. F., Colwell, J., Hendrix, A., Pryor, W., Shemansky, D., & West, R. 2006, *Science*, 311, 1422
- Hart, M. H. 1979, *Icarus*, 37, 351
- Heller, R., Leconte, J., & Barnes, R. 2011, *Astro. & Astrophys.*, 528, A27+
- Heng, K., & Vogt, S. S. 2011, *Mon. Not. Roy. Astron. Soc.*, 415, 2145
- Henning, W. G., O'Connell, R. J., & Sasselov, D. D. 2009, *Astrophys. J.*, 707, 1000
- Holden, J. F., Summit, M., & Baross, J. A. 1998, *FEMS Microbiology Ecology*, 25, 33
- Hurford, T. A., Helfenstein, P., Hoppa, G. V., Greenberg, R., & Bills, B. G. 2007, *Nature*, 447, 292
- Hut, P. 1981, *Astro. & Astrophys.*, 99, 126
- Ibgui, L., & Burrows, A. 2009, *Astrophys. J.*, 700, 1921
- Ingersoll, A. P. 1969, *J. Atmos. Sci.*, 26, 1191
- Jackson, B., Barnes, R., & Greenberg, R. 2008a, *Mon. Not. Roy. Astron. Soc.*, 391, 237

- . 2009, *Astrophys. J.*, 698, 1357
- Jackson, B., Greenberg, R., & Barnes, R. 2008b, *Astrophys. J.*, 678, 1396
- . 2008c, *Astrophys. J.*, 681, 1631
- Jayne, S. R. 2001, *Geophys. Res. Lett.*, 28, 811
- Johnson, T. V., Cook, II, A. F., Sagan, C., & Soderblom, L. A. 1979, *Nature*, 280, 746
- Jones, H. R. A., Butler, R. P., Tinney, C. G., Marcy, G. W., Carter, B. D., Penny, A. J., McCarthy, C., & Bailey, J. 2006, *Mon. Not. Roy. Astron. Soc.*, 369, 249
- Joshi, M. 2003, *Astrobiology*, 3, 415
- Joshi, M. M., Haberle, R. M., & Reynolds, R. T. 1997, *Icarus*, 129, 450
- Kaltenegger, L., & Traub, W. A. 2009, *Astrophys. J.*, 698, 519
- Kasting, J. F. 1988, *Icarus*, 74, 472
- Kasting, J. F., & Pollack, J. B. 1983, *Icarus*, 53, 479
- Kasting, J. F., Whitmire, D. P., & Reynolds, R. T. 1993, *Icarus*, 101, 108
- Kelly, S. M., Nash, J. D., & Kunze, E. 2010, *J. Geophys. Res.*, 115, C06014
- Khaliullin, K. F., & Khaliullina, A. I. 2011, *Mon. Not. Roy. Astron. Soc.*, 411, 2804
- Khodachenko, M. L. et al. 2007, *Astrobiology*, 7, 167
- Kokubo, E., & Ida, S. 1998, *Icarus*, 131, 171
- Komabayashi, M. 1967, *J. Meteor. Soc. Japan*, 45, 137
- Koriski, S., & Zucker, S. 2011, *Astrophys. J.*, 741, L23
- Kundurthy, P., Agol, E., Becker, A. C., Barnes, R., Williams, B., & Mukadam, A. 2011, *Astrophys. J.*, 731, 123
- Lainey, V., Arlot, J.-E., Karatekin, Ö., & van Hoolst, T. 2009, *Nature*, 459, 957
- Lainey, V., Dehant, V., & Pätzold, M. 2007, *Astro. & Astrophys.*, 465, 1075
- Lambeck, K. 1977, *Royal Society of London Philosophical Transactions Series A*, 287, 545
- Lammer, H. et al. 2007, *Astrobiology*, 7, 185
- . 2010, *Astrobiology*, 10, 45
- Laver, C., de Pater, I., & Marchis, F. 2007, *Icarus*, 191, 749
- Lecar, M., & Aarseth, S. J. 1986, *Astrophys. J.*, 305, 564
- Leconte, J., Chabrier, G., Baraffe, I., & Levrard, B. 2010, *Astro. & Astrophys.*, 516, A64+
- Léger, A. et al. 2009, *Astro. & Astrophys.*, 506, 287
- . 2004, *Icarus*, 169, 499
- Levrard, B., Winisdoerffer, C., & Chabrier, G. 2009, *Astrophys. J.*, 692, L9
- Lin, D. N. C., Bodenheimer, P., & Richardson, D. C. 1996, *Nature*, 380, 606

- Lissauer, J. J. 1993, *Ann. Rev. Astron. & Astrophys.*, 31, 129
- . 2007, *Astrophys. J.*, 660, L149
- Lunine, J. I. et al. 2008, *Astrobiology*, 8, 875
- MacDonald, G. J. F. 1964, *Reviews of Geophysics and Space Physics*, 2, 467
- Mandell, A. M., Raymond, S. N., & Sigurdsson, S. 2007, *Astrophys. J.*, 660, 823
- Mardling, R. A., & Lin, D. N. C. 2002, *Astrophys. J.*, 573, 829
- Marty, B., & Yokochim, R. 2006, *Rev. Mineral. Geochem.*, 62, 421
- Matsumura, S., Peale, S. J., & Rasio, F. A. 2010, *Astrophys. J.*, 725, 1995
- Mayor, M. et al. 2009, *Astro. & Astrophys.*, 507, 487
- McArthur, B. E. et al. 2004, *Astrophys. J.*, 614, L81
- McEwen, A. S., Keszthelyi, L. P., Lopes, R., Schenk, P. M., & Spencer, J. R. 2004, *The lithosphere and surface of Io*, ed. Bagenal, F., Dowling, T. E., & McKinnon, W. B., 307–328
- Meadows, V. S., Barnes, R., & *et al.* in prep., *AsBio*
- Monteiro, H. 2010, *Bulletin of the Astronomical Society of Brazil*, 29, 22
- Murakami, M., Hirose, K., Yurimoto, H., Nakashima, S., & Takafuji, N. 2002, *Science*, 295, 1885
- Murray, C. D., & Dermott, S. F. 1999, *Solar system dynamics*, ed. Murray, C. D. & Dermott, S. F.
- Naef, D. et al. 2001, *Astro. & Astrophys.*, 375, L27
- Nakajima, S., Hayashi, Y.-Y., & Abe, Y. 1992, *J. Atmos. Sci.*, 49, 2256
- Neron de Surgy, O., & Laskar, J. 1997, *Astro. & Astrophys.*, 318, 975
- Nesvorný, D. 2011, *Astrophys. J.*, 742, L22
- Nutzman, P., & Charbonneau, D. 2008, *Pub. Astron. Soc. Pac.*, 120, 317
- Nycander, J. 2005, *J. Geophys. Res.*, 110, C10028
- O’Brien, D. P., Morbidelli, A., & Levison, H. F. 2006, *Icarus*, 184, 39
- Olson, P., & Christensen, U. R. 2006, *Earth and Planetary Science Letters*, 250, 561
- Peale, S. J., Cassen, P., & Reynolds, R. T. 1979, *Science*, 203, 892
- Pierrehumbert, R. T. 2010, *Principles of Planetary Climate*
- . 2011, *Astrophys. J.*, 726, L8+
- Pollack, J. B. 1971, *Icarus*, 14, 295
- Porco, C. C. et al. 2006, *Science*, 311, 1393
- Raymond, S. N., Mandell, A. M., & Sigurdsson, S. 2006, *Science*, 313, 1413
- Raymond, S. N., Quinn, T., & Lunine, J. I. 2004, *Icarus*, 168, 1

- Raymond, S. N., Scalo, J., & Meadows, V. S. 2007, *Astrophys. J.*, 669, 606
- Reid, I. N., & Hawley, S. L. 2000, New light on dark stars. Red dwarfs, low-mass stars, brown dwarfs., ed. Reid, I. N. & Hawley, S. L.
- Rodler, F., Del Burgo, C., Witte, S., Helling, C., Hauschildt, P. H., Martín, E. L., Álvarez, C., & Deshpande, R. 2011, *Astro. & Astrophys.*, 532, A31+
- Sada, P. V. et al. 2010, *Astrophys. J.*, 720, L215
- Scalo, J. et al. 2007, *Astrobiology*, 7, 85
- Seager, S., Deming, D., & Valenti, J. A. 2009, *Transiting Exoplanets with JWST*, ed. Thronson, H. A., Stiavelli, M., & Tielens, A., 123
- Seager, S., Kuchner, M., Hier-Majumder, C. A., & Militzer, B. 2007, *Astrophys. J.*, 669, 1279
- Segatz, M., Spohn, T., Ross, M. N., & Schubert, G. 1988, *Icarus*, 75, 187
- Segura, A., Walkowicz, L. M., Meadows, V., Kasting, J., & Hawley, S. 2010, *Astrobiology*, 10, 751
- Selsis, F., Kasting, J. F., Levrard, B., Paillet, J., Ribas, I., & Delfosse, X. 2007, *Astro. & Astrophys.*, 476, 1373
- Showman, A. P., & Polvani, L. M. 2011, *Astrophys. J.*, 738, 71
- Simpson, G. 1927, *Mem. Roy. Met. Soc.*, 11, 69
- Sotin, C., Grasset, O., & Mocquet, A. 2007, *Icarus*, 191, 337
- Spencer, J. R., Rathbun, J. A., Travis, L. D., Tamppari, L. K., Barnard, L., Martin, T. Z., & McEwen, A. S. 2000, *Science*, 288, 1198
- Stevenson, D. J. 2010, *Sp. Sci. Rev.*, 152, 651
- Strom, R. G., Terrile, R. J., Hansen, C., & Masursky, H. 1979, *Nature*, 280, 733
- Swift, D. C. et al. 2012, *Astrophys. J.*, 744, 59
- Tamuz, O. et al. 2008, *Astro. & Astrophys.*, 480, L33
- Tarter, J. C. et al. 2007, *Astrobiology*, 7, 30
- Tian, F. 2009, *Astrophys. J.*, 703, 905
- Touma, J., & Wisdom, J. 1994, *Astron. J.*, 108, 1943
- Tsiganis, K., Gomes, R., Morbidelli, A., & Levison, H. F. 2005, *Nature*, 435, 459
- Tyler, R. 2011, *Icarus*, 211, 770
- Tyler, R. H. 2008, *Nature*, 456, 770
- Udry, S. et al. 2007, *Astro. & Astrophys.*, 469, L43
- Valencia, D., Ikoma, M., Guillot, T., & Nettelmann, N. 2010, *Astro. & Astrophys.*, 516, A20
- Valencia, D., Sasselov, D. D., & O'Connell, R. J. 2007, *Astrophys. J.*, 665, 1413
- Veeder, G. J., Matson, D. L., Johnson, T. V., Blaney, D. L., & Goguen, J. D. 1994, *J. Geophys. Res.*, 99, 17095

- Vogt, S. S., Butler, R. P., Rivera, E. J., Haghighipour, N., Henry, G. W., & Williamson, M. H. 2010, *Astrophys. J.*, 723, 954
- von Bloh, W., Bounama, C., Cuntz, M., & Franck, S. 2007, *Astro. & Astrophys.*, 476, 1365
- Watson, A. J., Donahue, T. M., & Kuhn, W. R. 1984, *Earth Plan. Sci. Lett.*, 68, 1
- Watson, A. J., Donahue, T. M., & Walker, J. C. G. 1981, *Icarus*, 48, 150
- Weidenschilling, S. J., & Marzari, F. 1996, *Nature*, 384, 619
- Weinberg, N. N., Arras, P., Quataert, E., & Burkart, J. 2011, ArXiv e-prints
- West, A. A., Hawley, S. L., Bochanski, J. J., Covey, K. R., Reid, I. N., Dhital, S., Hilton, E. J., & Masuda, M. 2008, *Astron. J.*, 135, 785
- Wetherill, G. W., & Stewart, G. R. 1989, *Icarus*, 77, 330
- Williams, D. M., & Pollard, D. 2002, *International Journal of Astrobiology*, 1, 61
- Winn, J. N. et al. 2011, *Astrophys. J.*, 737, L18+
- Wordsworth, R. D., Forget, F., Selsis, F., Millour, E., Charnay, B., & Madeleine, J.-B. 2011, *Astrophys. J.*, 733, L48+
- Yoder, C. F. 1995, in *Global Earth Physics: A Handbook of Physical Constants*, ed. T. J. Ahrens, 1–+
- Zahn, J.-P. 1977, *Astro. & Astrophys.*, 57, 383
- Zahn, J.-P., & Bouchet, L. 1989, *Astro. & Astrophys.*, 223, 112
- Zechmeister, M., Kürster, M., & Endl, M. 2009, *Astro. & Astrophys.*, 505, 859

This 2-column preprint was prepared with the AAS L^AT_EX macros v5.2.

A. Relations for the inner edge of the habitable zone

The critical flux for the runaway greenhouse depends weakly on the acceleration due to gravity, g , in the planetary atmosphere. Flux is emitted to space from the level of optical depth of unity. The optical depth of a layer of absorbing gas depends to first approximation on the mass of the layer, so with higher g the pressure at the base of a constant mass layer will be higher. For the Simpson -Nakajima limit, the T - p structure of the atmosphere is the saturation vapor pressure curve, so higher p implies higher T and permits a higher critical flux. This positive relationship is offset to some extent by pressure-broadening of absorption, so at higher g (and higher p), less mass of water is required to provide an optical depth of unity (Pierrehumbert 2010; Goldblatt & Watson 2012).

Pierrehumbert (2010) derives a semi-analytical relationship for the critical flux due to the Simpson-Nakajima limit:

$$F_{\text{crit}} = A\sigma \left(\frac{l}{R \ln \left(P_{\star} \sqrt{\frac{\kappa}{2P_0 g}} \right)} \right)^4 \quad (\text{A1})$$

where l is the latent heat capacity of water, R is the universal gas constant, P_0 is the pressure at which the line strengths are evaluated, g is the gravitational acceleration in the planetary atmosphere. κ is a gray absorption coefficient and A is a constant of order unity; Pierrehumbert (2010) fits these to numerical runs of a radiative transfer code with $\kappa = 0.055$ and $A = 0.7344$.

$$P_{\star} = P_{\text{ref}} e^{\frac{l}{RT_{\text{ref}}}}, \quad (\text{A2})$$

where $T_{\text{ref}} = 273.13$ K and $P_{\text{ref}} = 610.616$ Pa are points on the saturation vapor pressure curve of water, taken as the triple point. This calculated limit is shown in Fig. 6.

For convenience, we use an empirical relationship for the moist greenhouse limit derived by Selsis et al. (2007):

$$l_{\text{in}} = (l_{\text{in}\odot} - a_{\text{in}}T_{\star} - b_{\text{in}}T_{\star}^2) \left(\frac{L_{\star}}{L_{\odot}} \right)^{1/2}. \quad (\text{A3})$$

The outer edge (not due to a desiccating greenhouse) can be expressed in a similar format as

$$l_{\text{out}} = (l_{\text{out}\odot} - a_{\text{out}}T_{\star} - b_{\text{out}}T_{\star}^2) \left(\frac{L_{\star}}{L_{\odot}} \right)^{1/2} \quad (\text{A4})$$

In these equations l_{in} and l_{out} are the inner and outer edges of the IHZ, respectively, in AU, $l_{\text{in}\odot}$ and $l_{\text{out}\odot}$ are the inner and outer edges of the IHZ in the solar system, respectively, in AU, $a_{\text{in}} = 2.7619 \times 10^{-5}$ AU/K, $b_{\text{in}} = 3.8095 \times 10^{-9}$ AU/K², $a_{\text{out}} = 1.3786 \times 10^{-4}$ AU/K, and $b_{\text{out}} = 1.4286 \times 10^{-9}$ AU/K² are empirically determined constants, and L_{\star} and L_{\odot} are the stellar and solar luminosity, respectively. $T_{\star} = T_{\text{eff}} - 5700$ K, where T_{eff} is the “effective temperature” of the star

$$T_{\text{eff}} = \left(\frac{L_{\star}}{4\pi\sigma R_{\star}^2} \right)^{\frac{1}{4}}, \quad (\text{A5})$$

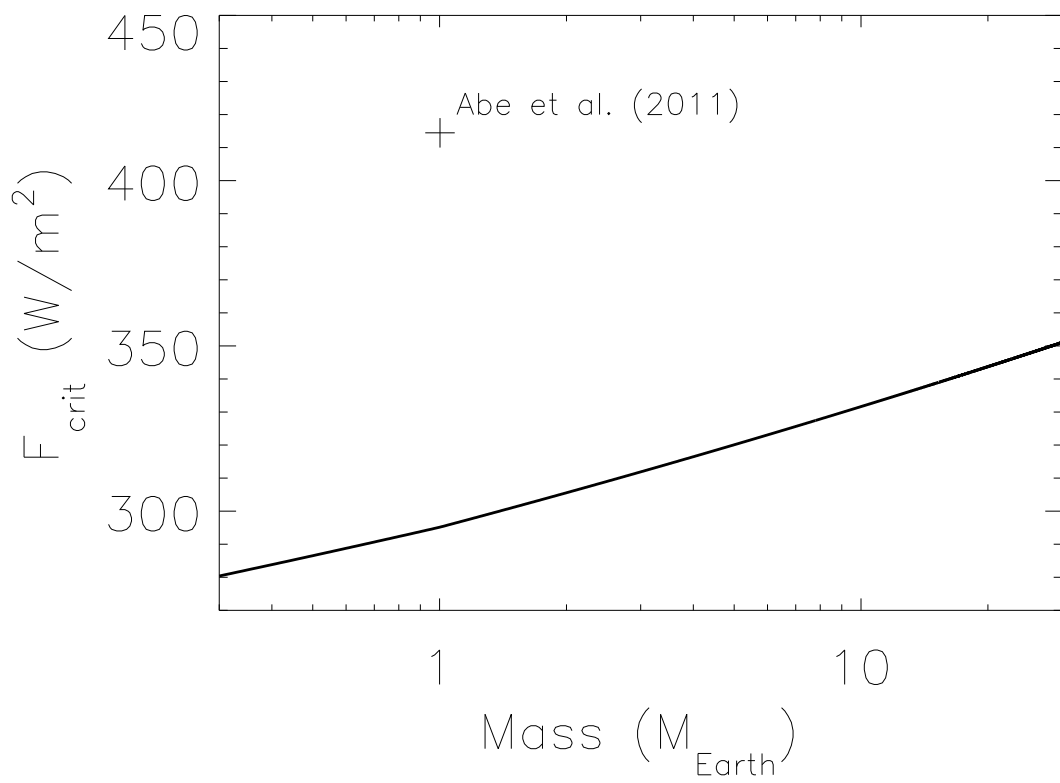


Fig. 6.— Surface flux required to trigger a runaway greenhouse (F_{crit}) as a function of planet mass. The solid line is the relation for wet planets from Pierrehumbert (2011), and the cross is the limit from Abe et al. (2011) for a dry planet.

where R_* is the stellar radius. Usually, however, the IHZ is couched in terms of the stellar mass M_* and a , and hence mathematical relationships between L_* , M_* and R_* are needed to produce such a relationship. Empirical and theoretical relations between these properties are reviewed in App. B.

The values of $l_{in\odot}$ and $l_{out\odot}$ are therefore the key parameters in the identification of the edges of the IHZ. We consider three criteria identified in Selsis et al. (2007): 1) 0% cloud cover, 2) 50% cloud cover, and 3) 100% cloud cover. Selsis et al. (2007) give values of $l_{in\odot}$ of 0.89, 0.72, and ~ 0.49 AU for the three possibilities, respectively. For the outer edge, Selsis et al. (2007) give values of $l_{out\odot}$ of 1.67, 1.95, and 2.4 AU, for the three cloud cover models, respectively. We arbitrarily choose the 50% cloud cover case to be the limits of the IHZ. This choice is the middle of the possibilities, and roughly corresponds to the cloud cover on the Earth.

However, as Selsis et al. (2007) note, “the effect of the spectral type on the albedo, included in [these equations] as a quadratic function of $(T_{\text{eff}} - 5700)$, was estimated only for a cloud-free atmosphere. Since the reflectivity of clouds is less sensitive to wavelength, this quadratic term may not be valid to scale the boundaries of the HZ for planets covered by clouds”. Furthermore, the assumption that Selsis et al. (2007) make that clouds do not affect the infrared flux from a planet at the inner edge of the habitable zone is not strong, so the cloudy results should be interpreted with caution. Furthermore, assumptions used in the models from which Selsis et al. (2007) derive their results assume fast planetary rotation, so it will not be a good approximation for most tidally-locked exoplanets.

Fig. 7 shows the range of the IHZ for the M dwarf mass range for the empirical relations presented in App. B. For very low-mass stars ($< 0.1 M_{\text{Sun}}$), the position of the IHZ may differ by 50% depending on the relationships invoked. However, for larger stars, the IHZ is mostly independent of the chosen mass-luminosity and mass-radius relationships.

B. Masses, Radii and Luminosities of M Dwarfs

In this appendix we review relationships between mass, radius, luminosity and effective temperature for M dwarfs ($M_* \leq 0.6 M_{\text{Sun}}$), and their effects on the limits of the IHZ. Measurements of these fundamental stellar properties are challenging and several studies have produced empirical and theoretical relations.

We first consider the mass-radius relation. We include empirical models by Gorda & Svechnikov (1999) (GS99), Reid & Hawley (2000) (RH00), Bayless & Orosz (2006) (BO06), as well as the theoretical models of Baraffe et al. (1998) (B98). This latter model is parameterized in terms of the metallicity as defined by astronomers:

$$[\text{Fe}/\text{H}] \equiv \log_{10}[\text{Fe}/\text{H}]_* - \log_{10}[\text{Fe}/\text{H}]_{\text{Sun}}, \quad (\text{B1})$$

in other words it is the difference between the ratio of iron to hydrogen in a star to that of the sun. B98 consider solar metallicity stars ($[\text{Fe}/\text{H}] = 0$) and sub-solar ($[\text{Fe}/\text{H}] = -0.5$).

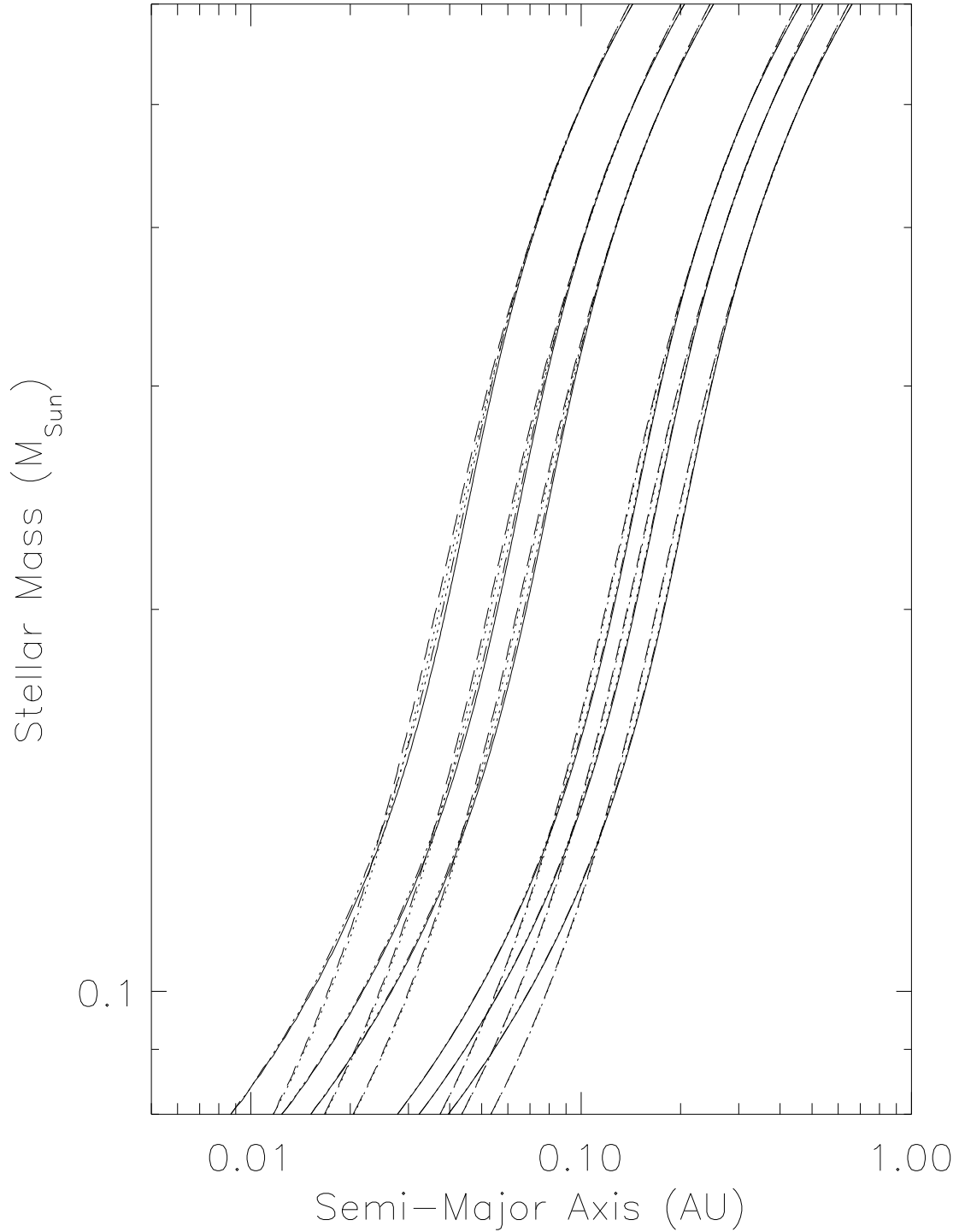


Fig. 7.— IHZ boundaries for different combinations of mass-radius and mass-luminosity relations, and using the three different cloud cover IHZ limits from Selsis et al. (2007). Except for the inner edge near $M_* = 0.2 M_{\text{Sun}}$,²⁹ the effective temperature does not affect the boundaries (note the numerous curves that are visible). Six combinations are plotted, but most are invisible as they are on top of each other. At low M_* , the more interior IHZ limits assume the RH00 mass-luminosity relationship, see App. B.

GS99 and BO06 present analytic fits that are shown in Table 1. For RH00, we take their data in Table 4.1 and derive a third-order polynomial fit, $y = b_0 + b_1x + b_2x^2 + b_3x^3$, using a Levenberg-Marquardt minimization scheme, and present the results in Table 1. The top two panels of Fig. 8 show the relationships graphically.

Next we examine the mass-luminosity relationships detailed in RH00, Scalo et al. (2007) (S07) and B98. For the former, we again fit their data with a third-order polynomial. The fits are listed in Table 1, and shown graphically in the bottom panels of Fig. 8.

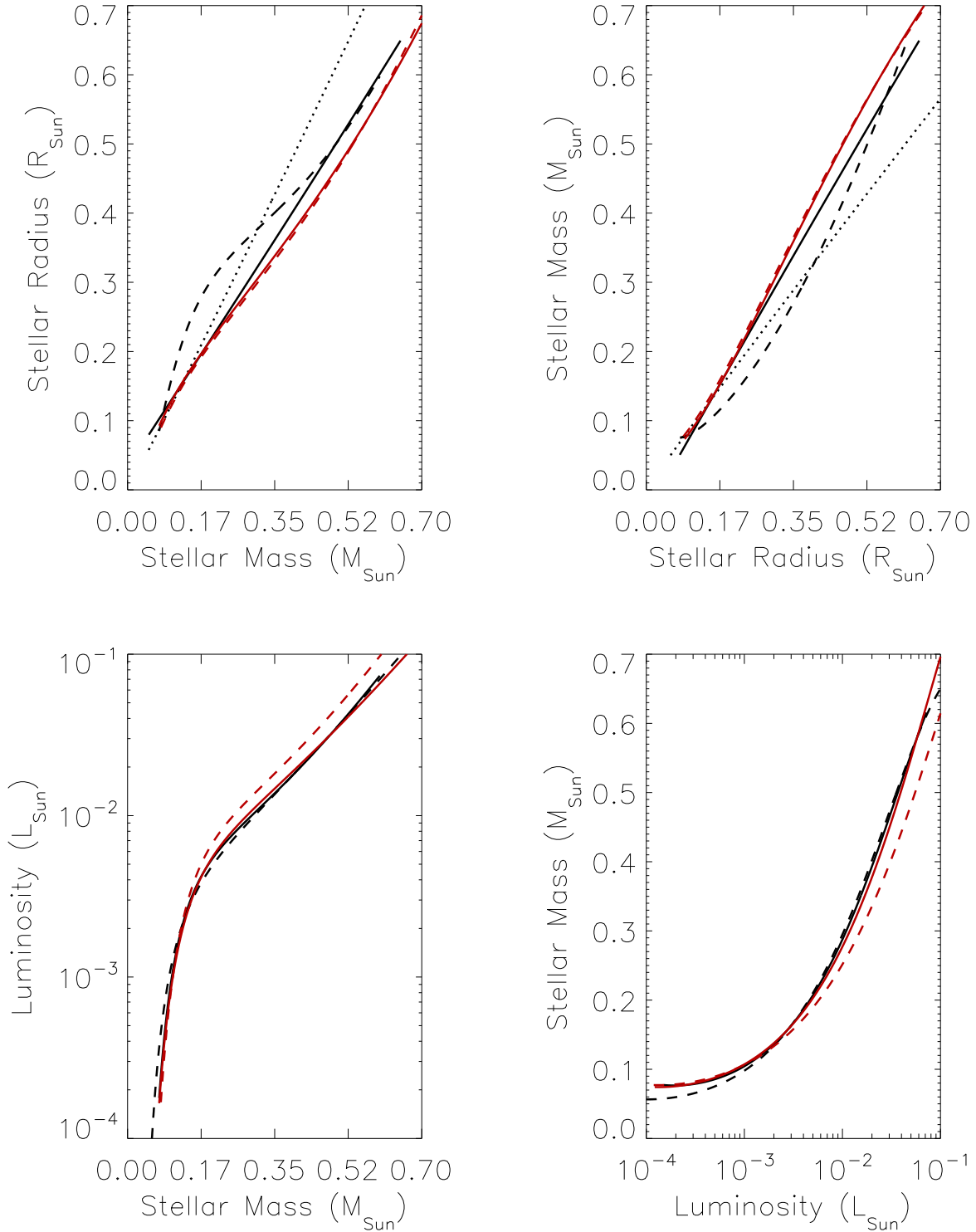


Fig. 8.— Scaling relations for M dwarfs. *Top*: Mass-radius relations. Black curves are empirical relations: solid from BO06, dashed from RH00, and dotted from GS99. Red curves are theoretical curves from B98: solid assumes $[\text{Fe}/\text{H}] = 0$, dashed $[\text{Fe}/\text{H}] = -0.5$. *Bottom*: Mass-luminosity relations. Black curves are empirical relations: solid from RH00, and dotted from Scalo et al. (2007). Red curves are theoretical curves from B98: solid assumes $[\text{Fe}/\text{H}] = 0$, dashed $[\text{Fe}/\text{H}] = -0.5$.

Table 1: Scaling Relations for M Dwarfs

x	y	b_0	b_1	b_2	b_3	χ^2	Ref.
$\log_{10}\left(\frac{M_*}{M_{\text{Sun}}}\right)$	$\log_{10}\left(\frac{R_*}{R_{\text{Sun}}}\right)$	0.1	1.03	0	0	n/a	GS99
$\log_{10}\left(\frac{M_*}{M_{\text{Sun}}}\right)$	$\log_{10}\left(\frac{R_*}{R_{\text{Sun}}}\right)$	0.0128	2.185	3.1349	1.903	0.0136	RH00
$\frac{M_*}{M_{\text{Sun}}}$	$\frac{R_*}{R_{\text{Sun}}}$	0.0324	0.0374	0	0	n/a	BO06
$\log_{10}\left(\frac{M_*}{M_{\text{Sun}}}\right)$	$\log_{10}\left(\frac{R_*}{R_{\text{Sun}}}\right)$	0.0372	1.5	1.09	0.5361	1.72×10^{-4}	B98([Fe/H]=0)
$\log_{10}\left(\frac{M_*}{M_{\text{Sun}}}\right)$	$\log_{10}\left(\frac{R_*}{R_{\text{Sun}}}\right)$	0.0664	1.685	1.398	0.7139	4.38×10^{-4}	B98([Fe/H]=-0.5)
$\log_{10}\left(\frac{R_*}{R_{\text{Sun}}}\right)$	$\log_{10}\left(\frac{M_*}{M_{\text{Sun}}}\right)$	-0.0971	0.971	-2.501×10^{-5}	-1.34×10^{-5}	1.2×10^{-10}	GS99
$\log_{10}\left(\frac{R_*}{R_{\text{Sun}}}\right)$	$\log_{10}\left(\frac{M_*}{M_{\text{Sun}}}\right)$	0.1424	1.568	-0.2342	-0.5581	0.0331	RH00
$\frac{R_*}{R_{\text{Sun}}}$	$\frac{M_*}{M_{\text{Sun}}}$	-0.03477	1.071	-8.171×10^{-4}	-0.0412	2.83×10^{-9}	BO06
$\log_{10}\left(\frac{R_*}{R_{\text{Sun}}}\right)$	$\log_{10}\left(\frac{M_*}{M_{\text{Sun}}}\right)$	-0.03	0.507	-1.156	-0.5978	8.88×10^{-4}	B98([Fe/H]=0)
$\log_{10}\left(\frac{R_*}{R_{\text{Sun}}}\right)$	$\log_{10}\left(\frac{M_*}{M_{\text{Sun}}}\right)$	-0.0406	0.4537	-1.211	-0.6427	1.39×10^{-3}	B98([Fe/H]=-0.5)
$\log_{10}\left(\frac{M_*}{M_{\text{Sun}}}\right)$	$\log_{10}\left(\frac{L_*}{L_{\text{Sun}}}\right)$	0.2984	8.7116	11.562	6.241	0.0155	RH00
$\log_{10}\left(\frac{M_*}{M_{\text{Sun}}}\right)$	$\log_{10}\left(\frac{L_*}{L_{\text{Sun}}}\right)$	0.065	7.108	8.162	4.101	n/a	S07
$\log_{10}\left(\frac{M_*}{M_{\text{Sun}}}\right)$	$\log_{10}\left(\frac{L_*}{L_{\text{Sun}}}\right)$	0.0182	7.228	9.357	5.281	0.039	B98([Fe/H]=0)
$\log_{10}\left(\frac{M_*}{M_{\text{Sun}}}\right)$	$\log_{10}\left(\frac{L_*}{L_{\text{Sun}}}\right)$	0.4377	8.908	12.21	6.896	0.094	B98([Fe/H]=-0.5)
$\log_{10}\left(\frac{L_*}{L_{\text{Sun}}}\right)$	$\log_{10}\left(\frac{M_*}{M_{\text{Sun}}}\right)$	-0.3076	-0.51	-0.4504	-0.06852	2.87×10^{-3}	RH00
$\log_{10}\left(\frac{L_*}{L_{\text{Sun}}}\right)$	$\log_{10}\left(\frac{M_*}{M_{\text{Sun}}}\right)$	-0.3536	-0.5463	-0.4422	-0.06243	0.224	S07
$\log_{10}\left(\frac{L_*}{L_{\text{Sun}}}\right)$	$\log_{10}\left(\frac{M_*}{M_{\text{Sun}}}\right)$	-0.04	-0.1144	-0.2765	-0.045	0.039	B98([Fe/H]=0)
$\log_{10}\left(\frac{L_*}{L_{\text{Sun}}}\right)$	$\log_{10}\left(\frac{M_*}{M_{\text{Sun}}}\right)$	-0.03	5.09×10^{-3}	-0.2135	-0.0368	0.0145	B98([Fe/H]=-0.5)

C. Radii of Terrestrial Planets

In this appendix we review published studies which provide analytic formulae relating terrestrial planet mass and radius. Throughout the study we appealed to the relationship derived by Sotin et al. (2007), who considered two types of planets: Earth-like composition and “ocean planets” that are 50% H₂O by weight. The scaling relationship for the former is

$$\frac{R_p}{R_{\text{Earth}}} = \begin{cases} \frac{M_p}{M_{\text{Earth}}}^{0.306} & 10^{-2} M_{\text{Earth}} < M_p < M_{\text{Earth}} \\ \frac{M_p}{M_{\text{Earth}}}^{0.274} & M_{\text{Earth}} < M_p < 10 M_{\text{Earth}} \end{cases} \quad (\text{C1})$$

and for the latter

$$\frac{R_p}{R_{\text{Earth}}} = \begin{cases} 1.258 \frac{M_p}{M_{\text{Earth}}}^{0.302} & 10^{-2} M_{\text{Earth}} < M_p < M_{\text{Earth}} \\ 1.262 \frac{M_p}{M_{\text{Earth}}}^{0.275} & M_{\text{Earth}} < M_p < 10 M_{\text{Earth}} \end{cases} \quad (\text{C2})$$

Fortney et al. (2007) parametrize the radii ($M_p > 0.01 M_{\text{Earth}}$) in terms of the ratio of ice to rock, f_{ice} , or rock to iron, f_{rock} . They assume that these two combinations are the most likely for terrestrial exoplanets and derived the following relationships:

$$\frac{R_p}{R_{\text{Earth}}} = (0.0912 f_{ice} + 0.1603) \left(\log_{10} \frac{M_p}{M_{\text{Earth}}} \right)^2 + (0.330 f_{ice} + 0.7387) \log_{10} \frac{M_p}{M_{\text{Earth}}} + 0.4639 f_{ice} + 1.1193, \quad (\text{C3})$$

$$\frac{R_p}{R_{\text{Earth}}} = (0.0592f_{\text{rock}}+0.0975)(\log_{10} \frac{M_p}{M_{\text{Earth}}})^2 + (0.2337f_{\text{rock}}+0.4938) \log_{10} \frac{M_p}{M_{\text{Earth}}} + 0.3102f_{\text{rock}}+0.7932. \quad (\text{C4})$$

In these equation $f_{\text{ice}} = 1$ corresponds to a pure iceball, $f_{\text{ice}} = 0$ and $f_{\text{rock}} = 1$ to a pure rock (silicate) planet, and $f_{\text{rock}} = 0$ is a planet made of pure iron. Note that Eqs. (C3)–(C4) are analytic fits to complex models, and hence predict slightly different values for R_p for a planet made of rock ($f_{\text{ice}} = 0$ and $f_{\text{rock}} = 1$). The Earth has $f_{\text{rock}} = 0.67$ and hence Eq. (C4) becomes $R_p/R_{\text{Earth}} = 0.1372[\log_{10}(M_p/M_{\text{Earth}})]^2 + 0.6504 \log_{10}(M_p/M_{\text{Earth}}) + 1.0010$.

Valencia et al. (2007) considered planets in the range 1–10 M_{Earth} and parameterized the radius in terms of f_{ice} (see also Valencia et al. 2010). They find

$$\frac{R_p}{R_{\text{Earth}}} = (1 + 0.56f_{\text{ice}}) \frac{M_p}{M_{\text{Earth}}}^{0.262(1-0.138f_{\text{ice}})}. \quad (\text{C5})$$

Seager et al. (2007) consider a wide range of planetary compositions and develop a general, but complicated, mass-radius relationship. Although they developed several formulae, here we only present one. They found that by casting M_p and R_p in terms of “scaling values” all planets follow the following relationship:

$$\log_{10} r_s = k_1 + k_2 \log_{10} m_s - k_2 m_s^{k_3}, \quad (\text{C6})$$

where $k_1 = -0.20945$, $k_2 = 0.0804$, and $k_3 = 0.394$. The parameters m_s and r_s are the scaled mass and radii, respectively, and are defined as $m_s = m/m_1$ and $r_s = r/r_1$, where the denominators are a scaling factor that depends on composition and thermal effects. We will consider four compositions. For pure iron planets, $m_1 = 5.8 M_{\text{Earth}}$, and $r_1 = 2.52 R_{\text{Earth}}$. For pure rock (perovskite) planets, $m_1 = 10.55 M_{\text{Earth}}$, and $r_1 = 3.9 R_{\text{Earth}}$. For pure water planets, $m_1 = 5.52 M_{\text{Earth}}$ and $r_1 = 4.43 R_{\text{Earth}}$. Finally, for an Earth-like planet (30% iron, 70% perovskite), $m_1 = 6.41 M_{\text{Earth}}$ and $r_1 = 2.84 R_{\text{Earth}}$. Note that this formulation is only valid for $m_s < 4$.

The last relationship we review is that of Grasset et al. (2009), who cast their model in terms only of f_{ice} . Their formulation is complicated and rather than reproduce it here, the reader is referred to their paper. We do not include the recent models put forth by Swift et al. (2012), as they do not include formulae, but they do find their results are consistent with those of Fortney et al. (2007) and Valencia et al. (2010) for rock and iron planets.

In Fig. 9 we compare these relationships from 0.3 – 30 M_{Earth} , and for a variety of compositions. Not all the relationships span that mass range, nor do they encompass all compositions. Furthermore, although we group planets into four types, not all types are identical. For example, we labeled the Sotin et al. (2007) ocean planet as a “Water” planet, but it is only 50% water, while the other three are 100% water. Nonetheless, the plot shows that if only mass is known, the radius of a planet can only be known to a factor of 2–2.5 (of course, its terrestrial nature is also unlikely to be known). As tidal heating scales as R_p^5 , this translates to a difference in heating of 30–100, assuming identical Q or τ . Note that the solid red curve (Earth-like planet from Sotin et al. (2007)) has a typical shape for its

class, hence the results presented here do not vary much if a different model is chose, unless a significantly different composition is invoked.

D. Tidal Theory

For our calculations of tidal evolution, we employ “equilibrium tide” models, originally conceived by Darwin (1880). This model assumes the gravitational potential of the tide raiser can be expressed as the sum of Legendre polynomials (*i.e.* surface waves) and that the elongated equilibrium shape of the perturbed body is slightly misaligned with respect to the line which connects the two centers of mass. This misalignment is due to dissipative processes within the deformed body and leads to a secular evolution of the orbit as well as the spin angular momenta of the two bodies. As described below, this approach leads to a set of 6 coupled, non-linear differential equations, but note that the model is, in fact, linear in the sense that there is no coupling between the surface waves which sum to the equilibrium shape. A substantial body of research is devoted to tidal theory (*e.g.* Hut 1981; Ferraz-Mello et al. 2008; Efroimsky & Williams 2009; Leconte et al. 2010), and the reader is referred to these studies for a more complete description of the derivations and nuances of tidal theory. For this investigation, we will use the models and nomenclature of Heller et al. (2011), which are presented below.

D.1. The Constant Phase Lag Model

In the “constant-phase-lag” (CPL) model of tidal evolution, the angle between the line connecting the centers of mass and the tidal bulge is assumed to be constant. This approach has the advantage of being analogous to a damped driven harmonic oscillator, a well-studied system, and is quite commonly utilized in planetary studies (*e.g.* Goldreich & Soter 1966; Greenberg 2009). In this case, the evolution is described by the following equations

$$\frac{de}{dt} = -\frac{ae}{8GM_1M_2} \sum_{i \neq j} Z'_i \left(2\varepsilon_{0,i} - \frac{49}{2}\varepsilon_{1,i} + \frac{1}{2}\varepsilon_{2,i} + 3\varepsilon_{5,i} \right) \quad (\text{D1})$$

$$\frac{da}{dt} = \frac{a^2}{4GM_1M_2} \sum_{i \neq j} Z'_i \left(4\varepsilon_{0,i} + e^2 \left[-20\varepsilon_{0,i} + \frac{147}{2}\varepsilon_{1,i} + \frac{1}{2}\varepsilon_{2,i} - 3\varepsilon_{5,i} \right] - 4 \sin^2(\psi_i) [\varepsilon_{0,i} - \varepsilon_{8,i}] \right)$$

$$\frac{d\omega_i}{dt} = -\frac{Z'_i}{8M_i r_{g,i}^2 R_i^2 n} \left(4\varepsilon_{0,i} + e^2 \left[-20\varepsilon_{0,i} + 49\varepsilon_{1,i} + \varepsilon_{2,i} \right] + 2 \sin^2(\psi_i) \left[-2\varepsilon_{0,i} + \varepsilon_{8,i} + \varepsilon_{9,i} \right] \right)$$

$$\frac{d\psi_i}{dt} = \frac{Z'_i \sin(\psi_i)}{4M_i r_{g,i}^2 R_i^2 n \omega_i} \left([1 - \xi_i] \varepsilon_{0,i} + [1 + \xi_i] \{ \varepsilon_{8,i} - \varepsilon_{9,i} \} \right), \quad (\text{D2})$$

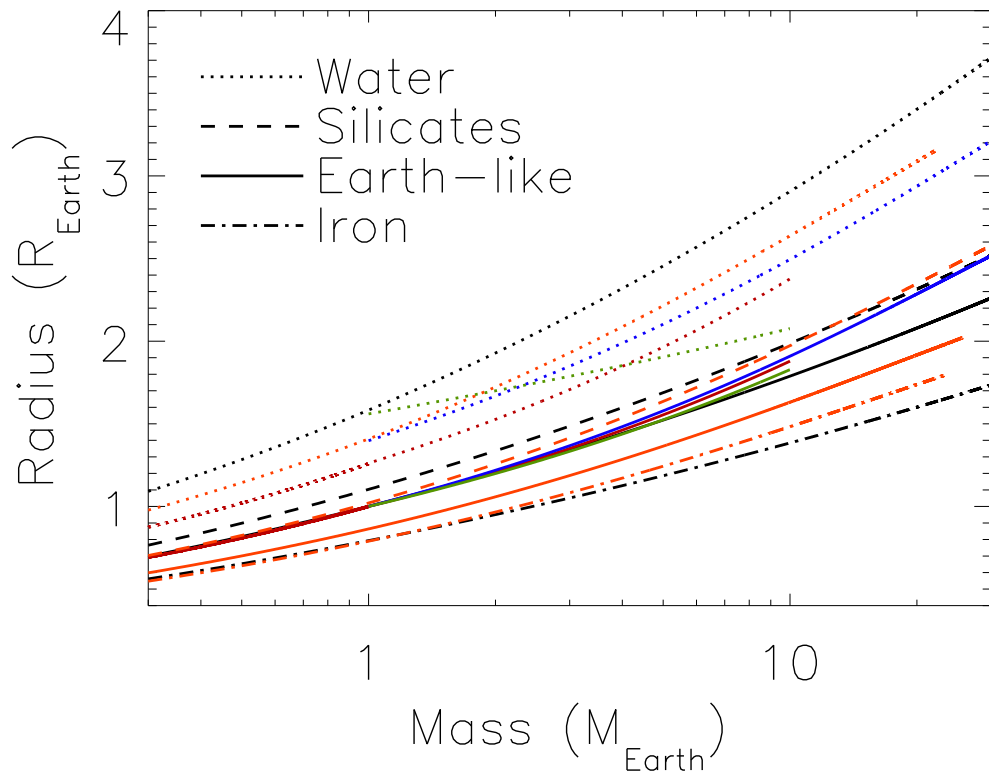


Fig. 9.— Mass-radius relationships for terrestrial planets of varying compositions. Solid curves assume a roughly Earth-like composition, dashed are all silicates, dotted are at least half water, and dot-dashed are pure iron. Black correspond to Fortney et al. (2007), red to Sotin et al. (2007), blue to Grasset et al. (2009), green to Valencia et al. (2007), and orange to Seager et al. (2007).

where e is eccentricity, t is time, a is semi-major axis, G is Newton's gravitational constant, M_1 and M_2 are the two masses, R_1 and R_2 are the two radii, ω_i are the rotational frequencies, ψ_i are the obliquities, and n is the mean motion. The quantity Z'_i is

$$Z'_i \equiv 3G^2 k_{2,i} M_j^2 (M_i + M_j) \frac{R_i^5}{a^9} \frac{1}{nQ_i}, \quad (\text{D3})$$

where $k_{2,i}$ are the Love numbers of order 2, and Q_i are the ‘‘tidal quality factors.’’ The parameter ξ_i is

$$\xi_i \equiv \frac{r_{g,i}^2 R_i^2 \omega_i a n}{GM_j}, \quad (\text{D4})$$

where i and j refer to the two bodies, and r_g is the ‘‘radius of gyration,’’ *i.e.* the moment of inertia is $M(r_g R)^2$. The signs of the phase lags are

$$\begin{aligned} \varepsilon_{0,i} &= \Sigma(2\omega_i - 2n) \\ \varepsilon_{1,i} &= \Sigma(2\omega_i - 3n) \\ \varepsilon_{2,i} &= \Sigma(2\omega_i - n) \\ \varepsilon_{5,i} &= \Sigma(n) \\ \varepsilon_{8,i} &= \Sigma(\omega_i - 2n) \\ \varepsilon_{9,i} &= \Sigma(\omega_i), \end{aligned} \quad (\text{D5})$$

with $\Sigma(x)$ the sign of any physical quantity x , thus $\Sigma(x) = +1 \vee -1 \vee 0$.

The tidal heating of the i th body is due to the transformation of rotational and/or orbital energy into frictional heating. The heating from the orbit is

$$\dot{E}_{\text{orb},i} = \frac{Z'_i}{8} \times \left(4\varepsilon_{0,i} + e^2 \left[-20\varepsilon_{0,i} + \frac{147}{2}\varepsilon_{1,i} + \frac{1}{2}\varepsilon_{2,i} - 3\varepsilon_{5,i} \right] - 4\sin^2(\psi_i) \left[\varepsilon_{0,i} - \varepsilon_{8,i} \right] \right),$$

and that from the rotation is

$$\dot{E}_{\text{rot},i} = -\frac{Z'_i \omega_i}{8n} \times \left(4\varepsilon_{0,i} + e^2 \left[-20\varepsilon_{0,i} + 49\varepsilon_{1,i} + \varepsilon_{2,i} \right] + 2\sin^2(\psi_i) \left[-2\varepsilon_{0,i} + \varepsilon_{8,i} + \varepsilon_{9,i} \right] \right).$$

The total heat in the i th body is therefore

$$\dot{E}_{\text{tide},i}^{\text{CPL}} = -(\dot{E}_{\text{orb},i} + \dot{E}_{\text{rot},i}) > 0. \quad (\text{D6})$$

The rate of evolution and amount of heating are set by three free parameters: Q , k_2 , and r_g . We discuss the ranges of these parameters below in App. D.4.

Goldreich (1966) suggested that the equilibrium rotation period for both bodies is

$$P_{eq}^{CPL} = \frac{P}{1 + 9.5e^2}. \quad (\text{D7})$$

Murray & Dermott (1999) present a derivation of this expression, which assumes the rotation rate may take a continuum of values. However, the CPL model described above only permits 4 “tidal waves”, and hence does not permit this continuum. In Fig. 10 we compare (D7) to the equilibrium values predicted by Eqs. (D1)–(D5) as a function of eccentricity for Gl 581 d (Mayor et al. 2009). As expected (D7) predicts a continuous range of periods, whereas our model (solid curve) does not. The jump at $e = \sqrt{1/19}$ occurs at the $\omega/n = 1.5$ transition, and nearly reaches the value predicted by (D7). The next phase jump at $e = \sqrt{2/19} \approx 0.32$ is not included in the CPL model, and hence it breaks down at larger values. However, at larger e values, coupling between waves and other non-linear effects may dampen the role of tides. Therefore the evolution at larger e predicted by the CPL model may not be qualitatively correct, however, we urge caution when interpreting CPL results above $e = 0.32$.

Thus, the CPL model can be considered from two perspectives. When modeling the evolution of a system, one should use the discrete spin values for self-consistency, *i.e.* as an initial condition, or if forcing the spin to remain tide-locked. However, if calculating the equilibrium spin period separately, the continuous value of Eq. D7 should be used. We refer to these rotations as “discrete states” and the “continuous state”. Note that this point marks a difference between our implementation of the CPL model, and that described in Heller et al. (2011).

D.2. The Constant Time Lag Model

The constant-time-lag (CTL) model assumes that the time interval between the passage of the perturber and the tidal bulge is constant. This assumption allows the tidal response to be continuous over a wide range of frequencies, unlike the CPL model. But, if the phase lag is a function of the forcing frequency, then the system is no longer analogous to a damped driven harmonic oscillator. Therefore, this model should only be used over a narrow range of frequencies, see Greenberg (2009). However, this model’s use is widespread, especially at high e , so we use it to evaluate tidal effects as well. This model predicts larger tidal heating and evolution rates at high e as any coupling between tidal waves is ignored. Therefore, the CPL and CTL models probably bracket the actual evolution.

The evolution is described by the following equations:

$$\frac{de}{dt} = \frac{11ae}{2GM_1M_2} \sum_{i \neq j} Z_i \left(\cos(\psi_i) \frac{f_4(e)}{\beta^{10}(e)} \frac{\omega_i}{n} - \frac{18}{11} \frac{f_3(e)}{\beta^{13}(e)} \right) \quad (\text{D8})$$

$$\frac{da}{dt} = \frac{2a^2}{GM_1M_2} \sum_{i \neq j} Z_i \left(\cos(\psi_i) \frac{f_2(e)}{\beta^{12}(e)} \frac{\omega_i}{n} - \frac{f_1(e)}{\beta^{15}(e)} \right) \quad (\text{D9})$$

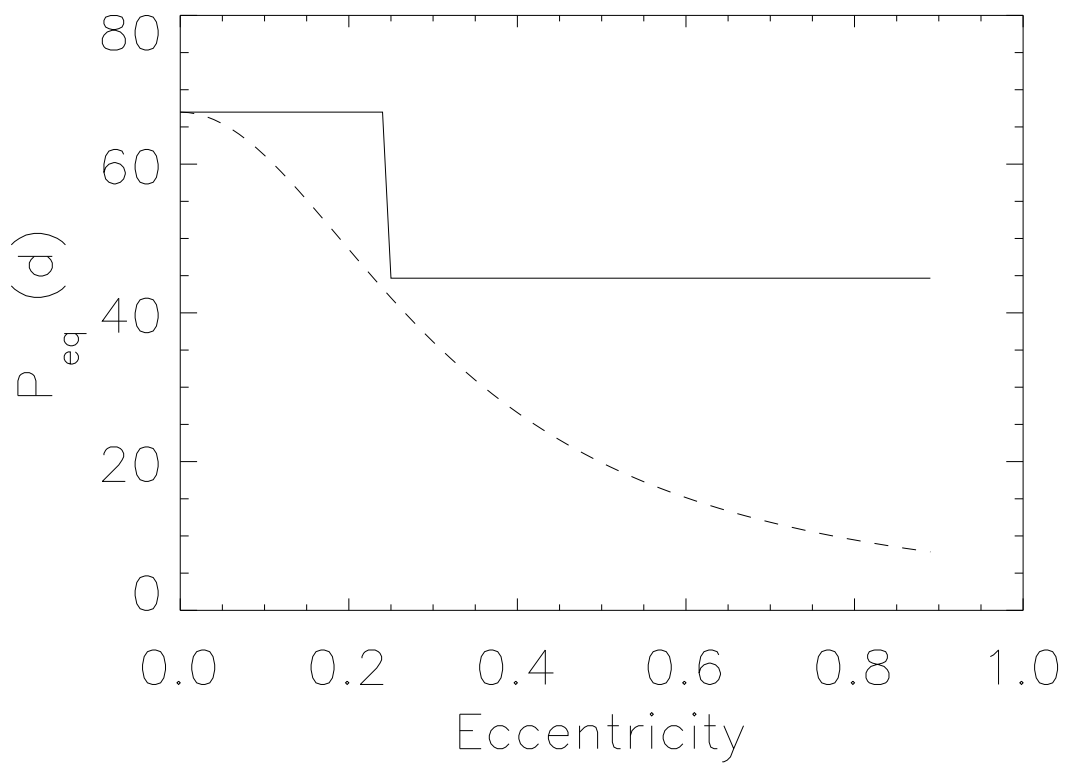


Fig. 10.— Comparison of the equilibrium spin periods in the CPL framework. The solid line is the value predicted by our model, Eqs. (D1)–(D5), the dashed is the “continuous” model of Goldreich (1966).

$$\frac{d\omega_i}{dt} = \frac{Z_i}{2M_i r_{g,i}^2 R_i^2 n} \left(2 \cos(\psi_i) \frac{f_2(e)}{\beta^{12}(e)} - [1 + \cos^2(\psi)] \frac{f_5(e)}{\beta^9(e)} \frac{\omega_i}{n} \right) \quad (\text{D10})$$

$$\frac{d\psi_i}{dt} = \frac{Z_i \sin(\psi_i)}{2M_i r_{g,i}^2 R_i^2 n \omega_i} \left(\left[\cos(\psi_i) - \frac{\xi_i}{\beta} \right] \frac{f_5(e)}{\beta^9(e)} \frac{\omega_i}{n} - 2 \frac{f_2(e)}{\beta^{12}(e)} \right) \quad (\text{D11})$$

where

$$Z_i \equiv 3G^2 k_{2,i} M_j^2 (M_i + M_j) \frac{R_i^5}{a^9} \tau_i, \quad (\text{D12})$$

and

$$\begin{aligned} \beta(e) &= \sqrt{1 - e^2}, \\ f_1(e) &= 1 + \frac{31}{2}e^2 + \frac{255}{8}e^4 + \frac{185}{16}e^6 + \frac{25}{64}e^8, \\ f_2(e) &= 1 + \frac{15}{2}e^2 + \frac{45}{8}e^4 + \frac{5}{16}e^6, \\ f_3(e) &= 1 + \frac{15}{4}e^2 + \frac{15}{8}e^4 + \frac{5}{64}e^6, \\ f_4(e) &= 1 + \frac{3}{2}e^2 + \frac{1}{8}e^4, \\ f_5(e) &= 1 + 3e^2 + \frac{3}{8}e^4. \end{aligned} \quad (\text{D13})$$

The tidal heating of the i th body is therefore

$$\dot{E}_{\text{tide},i}^{\text{CTL}} = Z_i \left(\frac{f_1(e)}{\beta^{15}(e)} - 2 \frac{f_2(e)}{\beta^{12}(e)} \cos(\psi_i) \frac{\omega_i}{n} + \left[\frac{1 + \cos^2(\psi_i)}{2} \right] \frac{f_5(e)}{\beta^9(e)} \left(\frac{\omega_i}{n} \right)^2 \right). \quad (\text{D14})$$

It can also be shown that the equilibrium rotation period for both bodies is

$$P_{eq}^{CTL}(e, \psi) = P \frac{\beta^3 f_5(e) (1 + \cos^2 \psi)}{2 f_2(e) \cos \psi}, \quad (\text{D15})$$

which for low e and $\psi = 0$ reduces to

$$P_{eq}^{CTL} = \frac{P}{1 + 6e^2}. \quad (\text{D16})$$

There is no general conversion between Q_p and τ_p . Only if $e = 0$ and $\psi_p = 0$, when merely a single tidal lag angle ε_p exists, then

$$Q_p \approx 1/(2|n - \omega_p| \tau_p), \quad (\text{D17})$$

as long as $n - \omega_p$ remains unchanged. Hence, a dissipation value for an Earth-like planet of $Q_p = 100$ is not necessarily equivalent to a tidal time lag of 638s, so the results for the tidal evolution will intrinsically differ among the CPL and the CTL model. However, both choices are common for the respective model.

D.3. Numerical Methods

The rates of change of the 6 parameters affected by tidal theory are all different. The orbital parameters tend to evolve several orders of magnitude more slowly than the planetary spin parameters, at least for the cases we are interested in. Therefore we implement a dynamical timestep scheme in our integration of tidal evolution. At the beginning of each timestep, we calculate the derivatives and set the timestep to

$$\Delta t = \eta \times \min\left(\frac{a}{da/dt}, \frac{e}{de/dt}, \frac{\omega_*}{d\omega_*/dt}, \frac{\psi_*}{d\psi_*/dt}, \frac{\omega_p}{d\omega_p/dt}, \frac{\psi_p}{d\psi_p/dt}\right), \quad (\text{D18})$$

where η is a constant, which we set to 0.01. We find that larger values of η , even up to unity, produce results similar with $\eta = 0.01$, but at our more conservative choice, we find almost no difference with even smaller value of η , *i.e.* the solution has converged. This implementation increases the speed of the code by several orders of magnitude in some cases. For example, if considering a planet with spin properties similar to the Earth at 0.01 AU, the timescale to damp out the obliquity is of order years, but the orbit evolves in millions of years (depending on e). Integrating this system for billions of years with a fixed timestep chosen to resolve the obliquity evolution will take many orders of magnitude more time than using this scheme. Dynamical timestepping is especially important for planets that merge with their host star (Jackson et al. 2009; Levrard et al. 2009).

In many cases, e and ψ can damp to arbitrarily small values, and hence de/dt and $d\psi/dt$ take on meaningless values. In some cases, their respective timescales as defined above can become very short, even though they are effectively 0. This situation destroys the speed advantage gained by utilizing (D18). We therefore set a floor for these values at 10^{-10} . When they reach this level, we set them to 0, and do not include them in the determination of Δt .

Finally, care must be taken as a planet approaches tidal locking. In many cases an integration will bounce back and forth above and below the equilibrium period. This possibility is a natural result of the discrete nature of numerical integration, but, again, can diminish the benefits of a dynamical timestep. Therefore, if a planet comes within 10% of the equilibrium period, we set the spin period to the equilibrium value. If the orbit is eccentric and evolving, after tidal locking, we force the planet to remain locked, *i.e.* the spin period obeys Eqs. (D7) or (D15).

D.4. Tidal Response in Celestial Bodies

Exoplanets are expected to have an even wider diversity of compositions and structures than those in our Solar System (see Raymond et al. 2004; Léger et al. 2004; O’Brien et al. 2006; Bond et al. 2010), thus their response to tidal processes probably varies greatly. We therefore choose to keep our model simple and set $k_2 = r_g = 0.5$ for all planets.

The Earth is the only body in the Solar System with a significant amount of water on its surface, and is also the planet with the most detailed picture of its tidal processes. Tidal

dissipation in the Earth’s ocean was directly measured from *TOPEX* and *Poseiden* satellite data by Egbert & Ray (2000) who found that 50–75% of dissipation occurs in and around shallow seas, with the remainder in the open ocean, presumably due to turbulence caused by topography. Recent computer simulations have successfully reproduced this observation (Jayne 2001; Nycander 2005; Kelly et al. 2010). For a more complete treatment of this process, consult Garrett & Kunze (2007). Therefore dissipation in planetary oceans is a complex function of continental shapes, sea floor topography and the forcing frequency.

Lunar Laser Ranging, in which the timing of laser pulses bounced off the Moon is measured, has provided very precise measurements of the rate of the Moon’s recession from the Earth (Dickey et al. 1994). If this recession is due only to tidal dissipation within the Earth, than the Earth’s tidal quality factor is $Q_{Earth} = 12$ (Yoder 1995). This value is lower than most measurements in the Solar System, which are more uncertain, see below. However, given the presence of surface oceans, this extra dissipation should be expected. On the other hand, extrapolating backward from the current orbital expansion rate and employing the CPL model, one finds the Moon was at the Earth’s surface ~ 2 Gyr ago (MacDonald 1964). The moon-forming impact has been dated to about 4.5 Gyr ago, and hence the Earth’s current Q appears too low. This discrepancy may be explained by 4 possibilities: 1) The current Q is anomalously low, and in the past different continental configurations and/or ocean floor topography did not permit such a high dissipation, 2) The tidal effects are a function of frequency, and as the Earth’s rotation has slowed, the dissipation rate has increased, 3) Perturbations from other planets affected the evolution (Ćuk 2007), or 4) Linear theory is oversimplified. Probably all of these possibilities play a role, and make the extension of tidal theory to an Earth-like exoplanet unreliable.

Measurements of the Martian dissipation function find $Q_{Mars} = 85.58 \pm 0.37$ (Bills et al. 2005) or $Q_{Mars} = 79.91 \pm 0.69$ (Lainey et al. 2007). The value for Mercury is $Q_{Mercury} < 190$, and for Venus it is $Q_{Venus} < 17$ (Goldreich & Soter 1966). Observations of Io imply $Q_{Io} < 100$ (Peale et al. 1979; Segatz et al. 1988), while the Moon lies at $Q_{Moon} = 26.5 \pm 1$ (Dickey et al. 1994). These measurements indicate a similar order of magnitude for the tidal dissipation function of all desiccated bodies in the Solar System.

Tidal effects on Venus may be particularly complicated due to its large atmosphere. The rotation rate of Venus is such that it always presents the same face to the Earth at inferior conjunction. Although this may be by chance due to Venus approaching tidal lock with the Sun, it has also been suggested that at some point in the past thermal atmospheric tides could have provided an equal but opposite torque than that from the rocky component. If that occurred, the torque from the Earth could dominate and spin-lock Venus (Gold & Soter 1969). More recent and detailed work has shown that this interaction can be significant and permits chaotic spin evolution that eventually settles into 1 of 4 possible states (Correia & Laskar 2001). Although a large atmosphere can play a significant role in the evolution of terrestrial planets (Correia & Laskar 2003), we ignore their effect here due to the large number of unknowns for an exoplanet.

In real bodies, Q is a function of the bodies’ rigidity μ , viscosity η , and temperature T

(Segatz et al. 1988; Fischer & Spohn 1990). A comprehensive tidal model would couple the orbital and structural evolution of the bodies since small perturbations in T can result in large variations in Q (Segatz et al. 1988; Mardling & Lin 2002; Efroimsky & Lainey 2007). Henning et al. (2009) sum up estimates for Q and the Love number of degree 2, k_2 , for planets in the solar system. They find $k_2 = 0.3$ and $Q = 50$ the most reasonable choice for an Earth-like planet.

The tidal properties of stars are about as poorly constrained as for planets. The primary constraint comes from the distribution of orbits of binary stars (*e.g.* Zahn 1977), whose orbits are circularized by the tidal interaction. However, for the closest binaries, where the tidal effects are strongest, and one might think the constraints the tightest, the situation is complicated by the early phases of stellar evolution (Zahn & Bouchet 1989), in which stellar radii contract rapidly. As the radius enters the tidal evolution at the fifth power, the radial contraction is a major effect. Recently Khaliullin & Khaliullina (2011) revisited this point and found that, although radial contraction does play a major role, they were unable to combine models of the equilibrium tide and radial contraction to match observations. Weinberg et al. (2011) tested the linear theory against non-linear models and found that in general the linear theory does not capture the physics of the more sophisticated approach. These studies demonstrate that there still exist serious problem with the linear theory, and quantitative discrepancies exist. However, it does qualitatively model the relevant physics, and allows wide sweeps of parameter space to be a computationally tractable problem. We therefore continue to use it, but explicitly acknowledge that known weaknesses persist.

A wide range of values for the tidal quality factor and tidal time lag for stars are present in the literature, ranging from $Q_* = 10^4$ (Adams et al. 2011) all the way to $Q_* = 10^9$ (Matsumura et al. 2010), with many others finding intermediate values (*e.g.* Lin et al. 1996; Carone & Pätzold 2007; Jackson et al. 2008b, 2009; Ibgui & Burrows 2009). For the star we take an intermediate and typical value of $Q_* = 10^6$.